UNIVERSITY OF CALIFORNIA
SANTA CRUZ

METASTABILITY OF TREMOLITE AT HIGH PRESSURES AND TEMPERATURES

A thesis submitted in partial satisfaction
of the requirements for the degree of

MASTER OF SCIENCE

in

EARTH SCIENCES

by

Jason Ott

June 2020

The Thesis of Jason Ott

is approved:

_____

Professor Quentin Williams, Chair

_____

Professor Elise Knittle

_____

Assistant Professor Alexander L. Ayzner

_____

Quentin Williams

Acting Vice Provost and Dean of Graduate Studies

Table of Contents

List of Figures

List of Tables

Abstract

Metastability of Tremolite at High Pressures and Temperatures

Jason N. Ott

Tremolite ($Ca_2Mg_5Si_8O_{22}(OH)_2$), a hydrated calcium-bearing amphibole mineral, is a common constituent of subducting oceanic lithosphere and an important source of water for geological processes in subduction zones. Researchers have proposed that metastably preserved tremolite may figure prominently in intermediate depth earthquakes and conductivity anomalies in the deep Earth, yet the metastability of tremolite has remained largely unstudied. Here, we explore the response of the tremolite structure to high pressures (to 49 GPa) and temperatures (to 540 K) via Raman spectroscopy and single-crystal X-ray diffraction (to 39 GPa). In both studies, tremolite metastably persists to the highest pressures explored with no evidence that the structure undergoes a phase transition, however, plots of the *a/b* and *a/c* axial ratios and an F_E-f_E plot reveal changes in the compressional behavior of tremolite at pressures near 5 and 22 GPa. Concordance between the mode shifts of the hydroxyl stretching vibration in our Raman study and previous infrared spectroscopic results implies a minimal role of Davydov splitting in tremolite and strengthens the conclusion that no approach toward hydrogen-bond symmetrization occurs with increasing pressure in the tremolite structure. The axial compressibilities of each compressional regime of tremolite were determined by fitting of a third-degree Birch-Murnaghan equation of state to our compressional data, and the results demonstrate a

strong reduction in the compressional anisotropy of tremolite in high-pressure regimes in contrast to increasingly anisotropic axial compressibilities observed in the high-pressure phases of cummingtonite and grunerite. The persistence of *C2/m* tremolite throughout the pressure-range of these studies represents the largest known metastability range of any amphibole and implies a correlation between M4 site occupancy and phase stability. However, the decreasing pressure-shifts of the lattice modes in our Raman data above 39 GPa and dramatic stiffening of the axial compressibilities in compression regime III imply an approach toward structural instability/amorphization in tremolite above 40 GPa at ambient temperatures.

Acknowledgements

I wish to express my sincere gratitude to my advisor, Professor Quentin Williams, whose guidance throughout this project has been without peer: many were the times that his encyclopedic knowledge of the overlapping disciplines that comprise mineral physics helped me break through the barriers I encountered during the experiments, analysis, and writing stages of this thesis. I also wish to thank the other members of my master's thesis reading committee, Professor Elise Knittle and Assistant Professor Alexander L. Ayzner, both of whom have been wonderful mentors and invaluable resources during my graduate studies program. Finally, I would like to extend a special thank you to my fellow students and researchers in the mineral physics laboratory: Dr. Cara Vennari, Genesis Berlanga, Garrett Zeff, and Ali Fuat Yuvali. It has been inspirational to share ideals with and learn from each of you over the last two years.

The text of this thesis includes a reprint of the following previously published material: Springer Nature: Physics and Chemistry of Minerals: Raman Spectroscopic Constraints on Compression and Metastability of the Amphibole Tremolite at High Pressures and Temperatures, Jason N. Ott and Quentin Williams, advance online publication, 9 May 2020 (doi: 10.1007/s00269-020-01095-6). The co-author listed in this publication directed and supervised the research which forms the basis for the thesis. I wish to thank Dr. Elise Knittle for helpful comments in the preparation of the published manuscript, Dr. Bora Kalkan at the Advanced Light Source and Dan

Sampson at UCSC for experimental support, and Dr. Thomas Duffy and a reviewer for helpful and constructive reviews.

The second chapter of this thesis is a manuscript in development for publication of work performed in collaboration with other co-authors in addition to my advisor, Professor Quentin Williams, and I wish to acknowledge their contributions to the work at this time: Dr. Bora Kalkan, the beamline scientist at the high-pressure beamline of the Advanced Light Source collected the ambient conditions tremolite single-crystal diffraction data and indexed/reduced the data, and also contributed to the experimental details section in the manuscript. I was the experimental lead during the collection of the high-pressure single-crystal diffraction data at the Advanced Light Source with a team composed of Dr. Kalkan, Genesis Berlanga, and Ali Yuvali. Indexing/refinement of the high-pressure data, data analysis and interpretation, and drafting of the manuscript were completed by myself with support, comments, and contributions from Dr. Kalkan and Professor Williams.

Funding for this work is provided by the National Science Foundation Division of Earth Sciences (NSF EAR-1620423), and by COMPRES, the Consortium for Materials Properties Research in Earth Sciences under NSF Cooperative Agreement EAR 1606856. Gas loading was performed at GeoSoilEnviroCARS (Sector 13), Advanced Photon Source (APS), Argonne National Laboratory. GeoSoilEnviroCARS is supported by the National Science Foundation - Earth Sciences (EAR-0217473), Department of Energy - Geosciences (DE-FG02-94ER14466) and the State of Illinois. Use of the APS was supported by the U.S.

Department of Energy, Office of Science, Office of Basic Energy Sciences, under Contract No. W-31-109-ENG-38. The Advanced Light Source (ALS) is supported by the Director, Office of Science, Office of Basic Energy Sciences, of the U.S. Department of Energy under Contract No. DE-AC02-05CH11231.

Dedication

I dedicate this work to my partner of these last 16 years, Jamie Brotzge, without whom I would never have found the courage to return to academia to pursue my love of science. Thank you for being there to cheer my accomplishments when I found success and ease my stress and frustration when it eluded me. Your friendship, support, and love are the greatest inspirations in my life.

Chapter 1

Raman Spectroscopic Constraints on Compression and Metastability of the Amphibole Tremolite at High Pressures and Temperatures

Jason N. Ott and Quentin Williams

1.1 Abstract:

Amphiboles, containing up to 2 wt% water in the form of hydroxyl units, contribute significantly to water transport into the deep lithosphere and upper mantle in subduction zones, where dehydration reactions make the water available for metasomatic processes and flux melting of the overlying mantle wedge. Here, we investigate the high-pressure and temperature behavior of the calcic end-member amphibole $Ca_2Mg_5Si_8O_{22}(OH)_2$-tremolite. Tremolite is characterized by Raman spectroscopy at pressures to ~49 GPa at room temperature, and at temperatures up to 540 K at ambient pressure. The behavior of the hydroxyl stretching vibration, concordant with previous infrared spectroscopic results, implies that the role of Davydov splitting in this amphibole is small, and the monotonically increasing mode shift of the hydroxyl peak under pressure indicates no approach toward hydrogen-bond symmetrization. As with a range of other hydroxyl-bearing minerals, the hydroxyl librations have slightly negative pressure-induced mode shifts. Intensity trends of Raman peaks that involve Ca-O displacements suggest changes in the calcium cation bonding environment above 10 GPa. The peak shifts of 18 modes are used to determine their isothermal and isobaric mode-Grüneisen parameters (γ_{iT} and

γ_{iP}). The intrinsic mode anharmonicities, calculated from the Grüneisen parameters, indicate largely quasi-harmonic internal mode vibrations while the lower frequency vibrations associated with cations display significant anharmonicity. The general topology of the tremolite structure remains metastable to ~50 GPa, and our work provides constraints on the metastability of amphiboles in subduction zones and the upper mantle, as well as the intrinsic crystallographic stability of the monoclinic amphibole structure.

1.2 Introduction:

Subduction zones are a key feature of plate tectonics, as the dynamics associated with subduction provides much of the driving force for plate motion. Hydrated mineral phases in oceanic lithosphere are carried to depth and undergo dehydration reactions that release water into the overlying mantle wedge driving flux melting and, ultimately, arc volcanism (Stern 2002; Pawley and Holloway 1993). Amphiboles are major rock-forming minerals in oceanic crust and depleted mantle that has been hydrothermally altered, and have been experimentally demonstrated to have thermodynamic stability ranges extending up to 2.5 GPa in materials with mid-ocean ridge basalt (MORB) and andesitic bulk compositions (Poli and Schmidt 1995; Schmidt and Poli 1998; Poli and Schmidt 2002); alkalic amphiboles may have high-temperature stabilities in mantle assemblages that exceed 12 GPa (e.g., Konzett and Fei 2000). Moreover, tremolite is often a product of serpentinite decomposition and may be important in the genesis of fluid overpressure associated with subducted slabs

(e.g., Tarling et al. 2019), and metastable entrainment of tremolite to depth could contribute to intermediate-depth earthquakes (Scamburelli et al. 2017). Dehydration reactions of amphiboles themselves are regarded as continuous over the P/T range of their breakdown, experimentally constrained to ~70-90 km of depth at equilibrium, and it is unclear the degree to which fluid is retained in the slab as this occurs (Schmidt and Poli 1998; Bell and Rossman 1992). Indeed, water involved in partial melting of the mantle wedge represents only a fraction of the water contained initially in minerals and as fluid in the down-going slab (Schmidt and Poli 1998), as depleted mantle wedge material also undergoes metasomatism driven by infiltrating water, as shown by the presence of the authigenic amphiboles tremolite and hornblende in xenoliths sourced from regions of arc magmatism (Kawamoto et al. 2013; Sakuyama and Koyaguchi 1984).

Amphiboles comprise a large, complex group of chemically diverse silicate minerals that can crystallize in the monoclinic and orthorhombic crystal systems. Amphiboles are inosilicates defined by the general formula $A_{0\text{-}1}B_2C_5T_8O_{22}W_2$ (Leake et al. 1997). Figure 1.1 shows the structure of an amphibole with monoclinic symmetry. Double-chain inosilicates are composed of interconnected corner-sharing tetrahedra, with the T-type cations in the T1 and T2 crystallographic sites extending along the direction of the crystallographic *c*-axis. These double-chains sandwich sheets of octahedrally coordinated C-type cations in the M1, M2, and M3 sites, forming the fundamental I-beam structural unit of amphiboles (Papike and Ross 1970; Law and Whittaker 1980). The I-beams form stacks along the *a*-axis, offset

from neighboring stacks along the *b*-axis direction, and the network of I-beams are interconnected by the B- and A-type cations in the M4 and A sites respectively. The

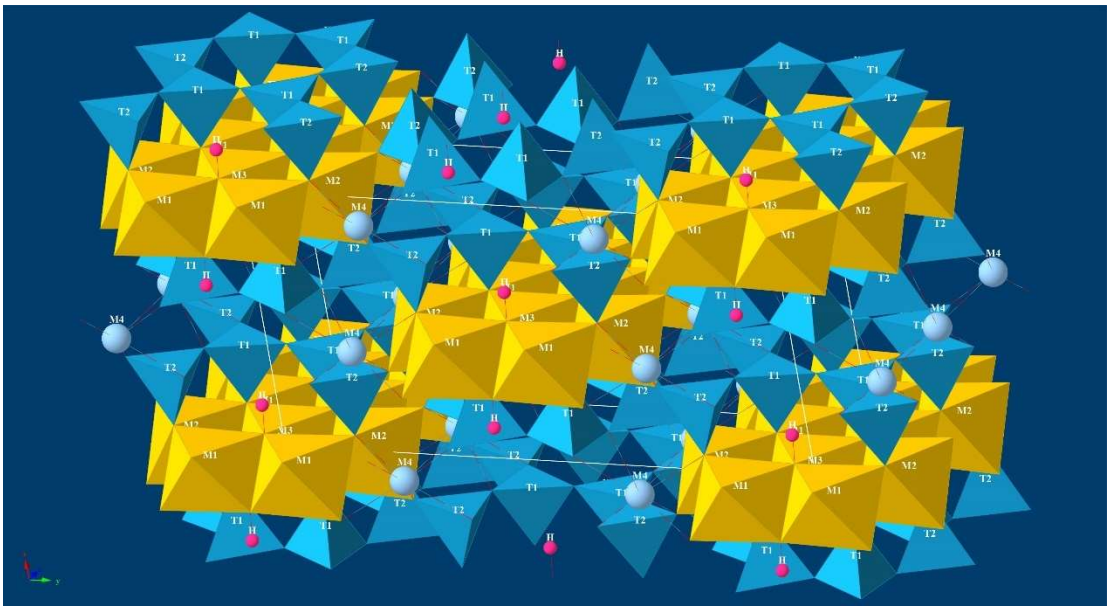

Figure 1.1: The general structure of an amphibole mineral such as tremolite, with monoclinic symmetry crystallizing in the C2/m space group. The x-y-z axes correspond to the a-b-c crystallographic axes

W-site of amphiboles, extending from the shared oxygen at each M1-M3-M1 junction into the space between the tetrahedral double-chains, is of particular interest as it is frequently occupied by water in the form of hydroxyl units, which comprise approximately 2% of the mineral by weight for fully hydroxylated stoichiometries (Hawthorne 1981). Amphiboles are subdivided into groups based on their crystal system, with further subdivisions based on the occupancy of the A, B, and C units of the general amphibole formula (Hawthorne 1981). Considered as a whole, the chemical and structural complexity of amphiboles present a myriad of questions

regarding the appearance of, the stability of, and the interactions between amphiboles and their environment.

Tremolite is a calcic amphibole with the end-member composition $Ca_2Mg_5Si_8O_{22}(OH)_2$ that crystallizes with monoclinic symmetry in the *C2/m* space group (Hawthorne 1981). Tremolite is frequently present in subduction zones in hydrothermally altered oceanic crust and depleted mantle material, metamorphosed pelagic sediments, and within regions of mantle wedges altered by metasomatism. Extensive studies have been made of tremolite at ambient conditions, along with a few studies at elevated temperatures, but there is a lack of experimental data on its response to the high pressures relevant to subduction zones. Raman spectroscopic studies at ambient conditions have been undertaken and peak assignments made by Blaha and Rosasco (1978), Huang (2002), Shurvell et al. (2001), and Apopei and Buzgar (2010). High-pressure infrared spectroscopy studies of the hydroxyl unit in amphiboles, including tremolite, reported a linear relationship between the pressure-induced frequency shift of hydroxyl stretching modes and their ambient frequency (Thompson et al. 2016). This extends to a correlation between the 1-bar stretching frequency and the tendency of the O-H bonds to weaken or strengthen with pressure corresponding to an increase or decrease of weak hydrogen bonding in the amphibole structure (Thompson et al. 2016). The elasticity of tremolite and other calcium bearing amphiboles were studied under ambient conditions by Brown and Abramson (2016) using Impulsive Stimulated Light Scattering (ISLS) to measure acoustic wave velocities. Their reported isotropically averaged adiabatic bulk modulus of 85 GPa for

tremolite agrees with other reported values, but interestingly, their findings indicate amphiboles to be more elastically anisotropic than previously proposed—with the lowest elastic moduli in the direction of the *a*-axis (Brown and Abramson 2016).

Comodi et al. (1991) conducted a high-pressure single-crystal X-ray diffraction (XRD) study that measured the compressibility and reported high-pressure structural refinements on several amphiboles, including tremolite, up to 4.1 GPa. Comodi et al. reported a similar bulk modulus of 85 GPa for tremolite and concluded that the structural accommodation of pressure-induced compaction was anisotropic, and primarily accomplished by flattening of the typically bowed tetrahedral double-chains (along the *b*-axis), thereby reducing the basal oxygen A-site distance and increasing the unique angle β between the *a*- and *c*-axes (Comodi et al. 1991). Additionally, a high-temperature X-ray diffraction study of tremolite was performed at 673 K and 973 K to determine the thermal expansion coefficients and differential thermal expansion of the structure (Sueno et al. 1973). Tremolite was not observed to undergo any pressure- or temperature-induced phase transitions in these studies; however, other monoclinic amphiboles have been reported to undergo phase transitions at high pressures and temperatures. Several researchers have observed temperature-induced phase transitions in cummingtonite ($(Mg,Fe)_2Mg_5Si_8O_{22}(OH)_2$), which transforms from the $P2_1/m$ space group to the $C2/m$ space group at temperatures ranging from 240 K to 373 K depending upon the occupancy of the M4 sites (e.g., Prewitt et al. 1970; Sueno et al. 1972; Yang and Smyth 1996). Pressure-driven transitions from $C2/m$ to $P2_1/m$ symmetry were reported in cummingtonite at

~1.21 GPa (Yang et al. 1998) and grunerite ($(Mg,Fe)_2Fe_5Si_8O_{22}(OH)_2$) at ~3 GPa (Yang et al. 1998; Boffa Ballaran et al. 2000). The structural similarities between tremolite and these other monoclinic amphiboles suggest the possibility that a similar phase transition could occur in the tremolite structure under compression.

In this study, we explore the metastability of tremolite under pressure to ~50 GPa, and under high-temperatures to ~540 K using Raman spectroscopy with an experimental focus on the bonding environment of the hydroxyl unit and the M-site cations—that is the B- and C-type cations from the general amphibole formula. As the low-symmetry and local site distortions of tremolite make it a relatively poor Raman scatterer, no prior Raman study of tremolite has been conducted at high pressures. Vibrational peaks are assigned at ambient pressure and compared to the results of other studies and theoretical calculations for Raman-active vibrations as calculated by Caracas and Bobocioiu (2011). The peak shifts with increasing pressure are fit to second-degree polynomials while the shifts with increasing temperatures are fit linearly, and the parameters from these fits are used to determine the isothermal and isobaric mode-Grüneisen parameters, respectively. The objective of this study is to use the analysis of the Grüneisen parameters, the shifts of the vibrational modes with pressure, and peak character and intensity to predict phase transitions or structural changes in tremolite and to direct future work on the stability and metastability of amphiboles in subduction zones and the upper mantle.

1.3 Experimental Methods:

The tremolite used in this study is from the Crevoladossola marble, quarried in the Ossola Valley of the Novara province of Italy. The tremolite sample was characterized by single-crystal X-ray diffraction under ambient conditions at beamline 12.2.2 of the Advanced Light Source synchrotron—analysis of which determined the sample was crystallized in the *C2/m* monoclinic space group with unit cell parameters a = 9.2815(12) Å, b = 18.0467(8) Å, c = 5.2722(2) Å, *beta* = 104.585(6)°, and V = 904.36(10) Å^3 in excellent agreement with previous work on near end-member composition tremolite (e.g., Comodi et al. 1991; Yang and Evans 1996). The tremolite sample is free of calcite and dolomite inclusions, as none of the high-intensity calcite or dolomite bands appear in the Raman spectra collected during this study. Furthermore, in the hydroxyl stretching vibration range of the Raman spectra, only a single sharp, narrow (~12 cm^{-1} full width at half maximum) band is present, from which it can be inferred that the tremolite is extremely close to end-member composition: that is, there is no significant substitution of Fe^{2+} for Mg^{2+} in the M sites of the octahedral strip within the I-beam structural units of the crystals (Hawthorne and Ventura 2007).

Elongated crystals from a hand sample were crushed in an agate mortar and pestle, and several crystals of approximately 40 x 20 x 20 μm were selected. Reference spectra were taken at atmospheric pressure and temperature and compared to tremolite spectra R150094 and R050498 from the RRUFF database to confirm the sample identity (Lafuente et al. 2015). High-pressure spectra were taken on multiple

runs over a pressure range from atmospheric to 48.7 GPa. High-temperature spectra were collected from 294 K to 540 K.

To collect spectra at high pressures, tremolite samples were loaded into a Princeton-type symmetric diamond anvil cell (DAC) with 350 μm culet diamond anvils. A 250 μm thick rhenium gasket was pre-indented to 50 μm thickness, and a circular 150 μm diameter sample chamber was drilled with a laser-milling system. After the sample chamber was drilled, residue from the laser milling process was removed initially by hand, followed by ultrasonic cleaning with a diluted cleaning solution and again with deionized water. The gasket was mounted to the piston-side diamond anvil, and several small ruby crystals (< 20 μm diameter) were loaded with a single tremolite crystallite that was mounted in the center of the piston-side diamond. Crystals were mounted with the *c*-axis parallel to the diamond culets in each experimental run, as all tremolite samples were elongated in the *c*-direction but consistently cleaved to much smaller dimensions in the *a*- and *b*-directions. Multiple sample runs were loaded using a 16:3:1 methanol-ethanol-water solution (Me-Eth-H_2O) as a pressure transmitting medium, and one sample was loaded in neon, as it has been shown to be a close-to-hydrostatic pressure medium to pressures near 50 GPa (Klotz et al. 2009). Spectral features collected from the sample loaded in neon were generally much sharper than corresponding features of the samples loaded in Me-Eth-H_2O. After allowing time for sample equilibration with each change in pressure, pressure measurements were determined by ruby fluorescence spectroscopy, with the R1 peak being fit, and the calibration of Mao et al. (1986) applied to its location.

Data at high temperatures were collected by placing both the tremolite crystal and a silicon calibrant into sample wells machined into copper mounted on a Peltier thermoelectric heating/cooling element. The sample wells were enclosed in a vacuum chamber during the variable temperature experiment. Target temperatures were set by use of a current controller equipped with a thermocouple in contact with the sample well. After allowing time for sample equilibration with each change in temperature, the temperature measurements were made using a calibration of the silicon (Si) Raman peak to room temperature of 294 K and calculations of the Si peak shift after Widulle et al. (2001).

Ruby fluorescence spectra and Raman spectra were collected using a Horiba Labram HR Evolution Raman Spectrometer utilizing an x50 LWD objective lens and a 1200 gr/mm grating with 532 and 633 nm excitation lasers for ruby fluorescence and Raman spectra respectively. Raman spectra were acquired over the spectral range of 50-1200 cm^{-1}, and 3500-3800 cm^{-1} with a spectral resolution of ~1 cm^{-1}. Acquisition times ranged from 30-120 seconds, and spectra were averaged over 5-8 accumulations to maximize the signal to noise ratio while avoiding saturation of the CCD by fluorescence and allowing the elimination of cosmic rays from individual acquisitions. This tremolite sample exhibits the strong fluorescence that is typical of amphiboles (e.g., Wang et al. 1988), and this appears as broad bands underlying the Raman signal that obscure and can even completely mask the lower-intensity regions of the tremolite Raman spectrum. Therefore, post-processing of the spectra was performed with Horiba Scientific's LabSpec 6 software: this consists of polynomial

smoothing of the signal through the application of the Savitsky-Golay algorithm (Savitzky and Golay 1964) and baseline subtraction. Peak fit calculations were made using Gaussian-Lorentzian combination peak shapes. Data collection also demonstrated substantial anisotropy in some of the Raman vibrations, leading to difficulty tracking some of the peak shifts over the pressure range explored. As the *c*-axis of the sample was oriented perpendicular to the excitation source, the hydroxyl peaks were especially difficult to resolve, and frequent reorientation of the DAC was required during data collection to collect high-quality spectra.

1.4 Results and Discussion:

Factor group analysis of the tremolite structure yields 61 Raman active vibrations with only two symmetry types, A_g (29) and B_g (32), as illustrated by the entry for tremolite in the WURM database (Caracas and Bobocioiu 2011). The Raman spectra collected during the high-pressure experiments resolved mode shifts for 21 vibrations over much or all of the pressure range investigated. Crystal orientation effects and differences in background between the samples loaded in Me-Eth-H_2O and Ne pressure media resulted in some peaks only being resolved during one of the sample runs (Figure 1.2). However, as low-pressure peak locations and mode-shifts were consistent for Raman peaks present in runs with both pressure media, results were considered as a single dataset during analysis. The observed vibrations can be divided into several general groups: 10 lattice modes, 6 vibrational modes associated primarily with cation-oxygen interactions, 2 libration modes of the

Figure 1.2: Pressure-induced mode-shifts of the Raman spectra of tremolite to ~50 GPa for multiple sample loadings with Me-Eth-H_2O or Ne as the pressure medium. Error bars for peak locations are smaller than the markers in the plot due to the proximity of the ruby pressure standards to the Raman spectra sampling locations. The mode shifts for spectra in the Me-Eth-H_2O medium diverge from those in the Ne medium above ~15 GPa due to increasing rigidity of Me-Eth-H_2O relative to Ne (see text). All pressure-induced shifts are monotonically positive, with the exception of the 2 libration modes (with ω_0 values of 582 and 599 cm^{-1}), which display small, negative pressure shifts. The translational vibrations of the cation-oxygen bonds (ω_0 between 278 and 439 cm^{-1}) exhibit complex behavior above ~12 GPa

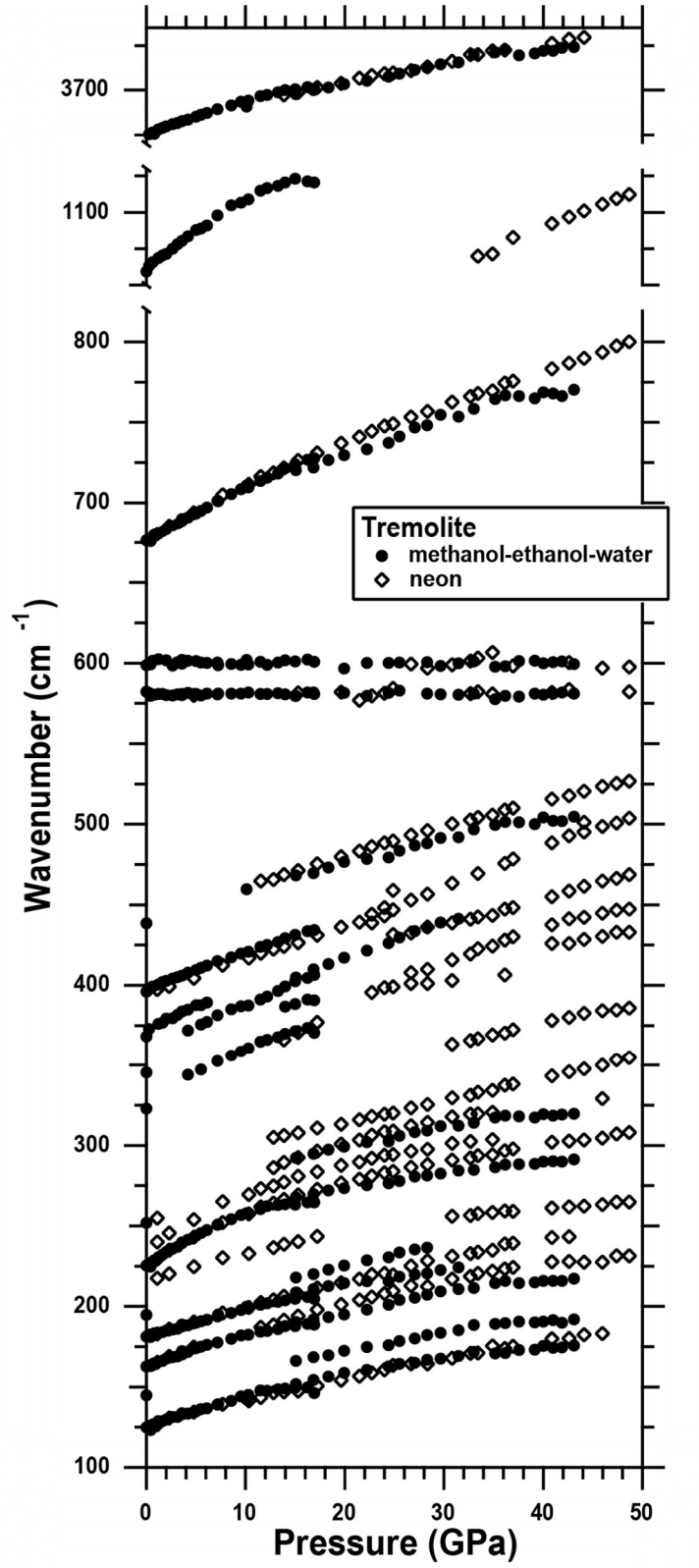
Tremolite
methanol-ethanol-water
neon
Wavenumber (cm -1)
Pressure (GPa)
3700
1100
800
700
600
500
400
300
200
100
0
10
20
30
40
50

hydroxyl units, 2 internal vibrations of the SiO_4 tetrahedral chains, and the single hydroxyl stretching vibration. Figure 1.3 shows representative spectra of tremolite with intensities that have been normalized to the highest intensity peak (the inter-tetrahedral mode located at ~676 cm^{-1} at ambient pressure) and illustrates the pressure shifts of the Raman modes from ambient pressure to ~41 GPa. Raman spectra of the high-temperature measurements (which were also intensity-normalized) allow thermal mode shifts for 18 vibrations to be tracked: 7 lattice modes, 5 cation-oxygen interaction vibrations, 1 libration mode of the hydroxyl unit, 4 internal vibrations, and the hydroxyl stretching vibrational mode. The temperature sensitivity of the vibrational modes is much smaller in magnitude than the response to changes in pressure, as shown by the lattice modes of tremolite at 294 and 540 K in Figure 1.4. Several different vibrational modes are resolvable in the high-pressure experiments relative to the modes observed in the high-temperature experiments: this difference is attributable to orientation effects of the crystals, and variable background signatures from the different experimental apparatuses in the two sets of experiments—nevertheless, a subset of 13 modes are resolved in both the high-pressure and high-temperature spectra.

Analysis of the difference between the ambient Raman peak locations from the theoretically derived peak locations of Caracas and Bobocioiu (2011) conducted using the Abinit software shows an average deviation of ~2% for the lattice and external modes, while the internal and hydroxyl peaks only deviate by ~0.5% on average. This result suggests that the frequency of vibrations with strong bonds

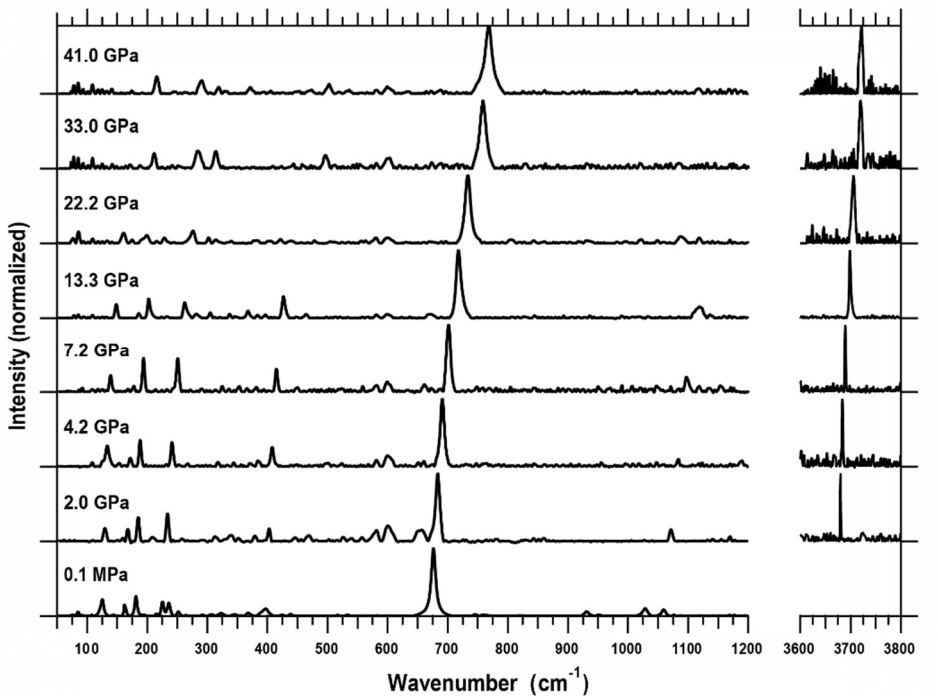

Figure 1.3: Representative spectra of tremolite as a function of pressure from 0.1MPa to 41 GPa in Me-Eth-H2O. The pressure-induced mode shifts for 18 peaks are resolved within the pressure range. Sample runs in Me-Eth-H¬2O were chosen for the representative spectra as pressure steps below 20 GPa were smaller on average than in Ne, allowing a better choice of spectra to illustrate the character of peaks and trend of pressure shifts

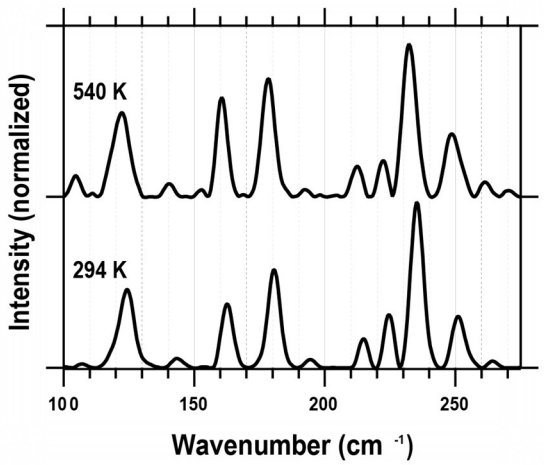

Figure 1.4: Representative spectra of tremolite lattice mode vibrations at 294 K and 540 K showing temperature-induced mode shifts

(higher frequencies) are theoretically predicted to a higher degree of accuracy than weak bonds. It would be of interest to determine if this trend extends to other materials theoretically treated in the WURM database that have been well-characterized by Raman spectroscopy.

1.4.1 Peak assignments:

Peak assignments for tremolite have been carried out for Raman studies performed at ambient conditions for modes lying within the 200-1200 cm^{-1} spectral range (Huang 2002; Shurvell et al. 2001; Apopei and Buzgar 2010). Using these previous experimental results and theoretical calculations presented in the WURM database (Caracas and Bobocioiu 2011), we make tentative peak assignments for the spectral range between 50-1200 cm^{-1} (Figure 1.2). The ambient pressure peaks at frequencies of 125, 145, 163, 181, 195, 218, 225, 239, and 252 cm^{-1} are in the range of lattice mode vibrations. The bands at 278, 307, 323, 345, 368, 396, and 439 cm^{-1} correspond predominantly to translational vibrations of the divalent cation-oxygen bonds (Mg^{2+} in the M1, M2, and M3 sites, Ca^{2+} in the M4 sites). The zero-pressure peaks at 582 and 599 cm^{-1} are assigned to hydroxyl librations. The remaining peaks in the 650-1200 cm^{-1} range are associated with the internal vibrations of the SiO_4 tetrahedral double-chains. The highest intensity peak in the tremolite spectrum, at 676 cm^{-1}, is the symmetric stretch of the Si-O-Si (ν_1) group. The symmetric stretch of the O-Si-O linkage (ν_s) is found at 932 cm^{-1}, and the 1028 and 1059 cm^{-1} peaks are the asymmetric stretches of the Si-O-Si unit (ν_{as}). Finally, the ambient pressure band at

3677 cm^{-1} is the stretching vibration of the hydroxyl unit (OH^-), as has been well-documented in previous studies using both Raman and infrared spectroscopy (e.g., Huang 2002; Thompson et al. 2016).

1.4.2 Hydroxyl stretch mode:

The pressure-induced shift in frequency of the Raman-active hydroxyl stretching vibration is plotted with the infrared spectroscopic hydroxyl shifts of Thompson et al. (2016) in Figure 1.5. The frequency of the hydroxyl stretching

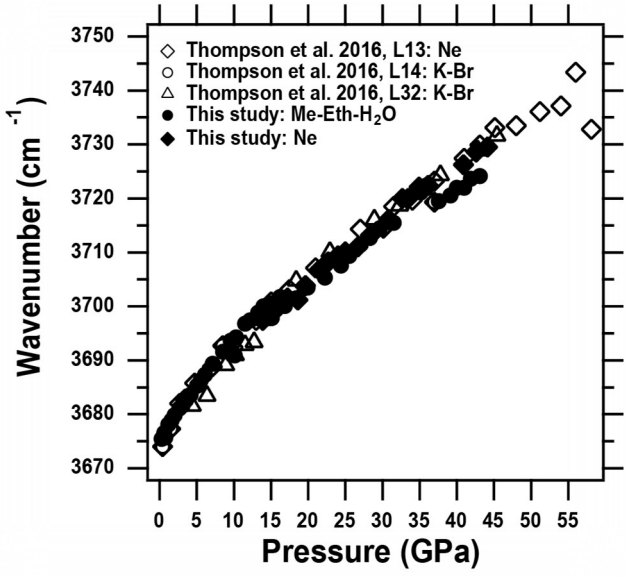

Figure 1.5: Comparison plot of the hydroxyl stretching vibration of tremolite at high pressure from infrared (Thompson et al. 2016) and Raman spectroscopy (this study)

vibration, with an ω_0 of 3677 cm^{-1} at standard conditions, signifies that the OH^- ions in the tremolite structure are not strongly hydrogen-bonded (Lutz 1995). The absolute location and pressure shift of the hydroxyl stretching vibration from our data are essentially indistinguishable from the infrared results of Thompson et al. despite the

different symmetry types of the vibrations (the infrared vibration is B_u symmetry, while the Raman vibration is A_g). Therefore, the effect of Davydov splitting, which is generated by inter-hydroxyl interactions within tremolite under pressure, is negligible. Described a different way, the in-phase vibrations of the hydroxyl units in the tremolite unit cell are essentially identical in frequency to the out-of-phase vibrations of the hydroxyls. This is perhaps not surprising, given the distance between the hydroxyls within the unit cell (Figure 1.1), but this lack of interaction persists to within ~1 cm^{-1} (or >0.03% of the total energy of the vibration) in measurements within neon to volume compressions of ~25% (Figure 1.5). In effect, the M1/M3 octahedral layer appears to effectively electrostatically shield the hydroxyls within the unit cell from one another. Additionally, the positive pressure-induced frequency shift of the hydroxyl vibration in both data sets strengthen previous findings that the hydrogen in tremolite becomes more localized with pressure: that is, there is no increase in hydrogen bonding (as would be manifested by a negative pressure shift), and hence no approach toward hydrogen-bond symmetrization. The O-H stretch also appears to shift largely linearly above ~10-15 GPa: no maximum is observed, as has been postulated to occur when the hydroxyl unit begins to impinge substantially into the six-membered silicate ring (Sheu and McMillan 1988).

1.4.3 Libration modes:

Many of the modes of tremolite monotonically increase in frequency up to 50 GPa (Figure 1.2). Notably, the mode shifts for the samples using Me-Eth-H_2O as the

pressure medium begin to diverge from the sample loaded in Ne above ~15 GPa as Me-Eth-H_2O becomes more non-hydrostatic near 15 GPa, while Ne remains quasi-hydrostatic to pressures approaching 50 GPa (Klotz et al. 2009). Of the peaks tracked through our pressure range, the hydroxyl libration modes are unique in that they display a small negative shift with increasing pressure. Small mode-shifts in hydroxyl librations in silicate minerals are well-precedented, having been observed in high-pressure studies of other silicate minerals including chondrodite (Williams 1992), clinozoisite and topaz (Bradbury and Williams 2003), talc and lawsonite (Scott et al. 2007), and muscovite, biotite, and phlogopite (Williams et al. 2012). The evidently small (and negative) pressure dependence of the hydroxyl libration in conjunction with the positive pressure shift (bond-length shortening) of the hydroxyl stretch may be attributed to variations in the electrical field induced by the neighboring anions and cations in the plane of the hydroxyl libration. With the pressure-induced decrease in hydrogen bonding, compaction of the cavity containing the hydroxyl units results in increased attractive and repulsive interactions between the surrounding ions and the hydrogen, and hence a vibrational motion of the libration that is progressively more distorted by compression from the ideal near-circular motion of an isolated hydroxyl libration (e.g., Shinoda and Aikawa 1997). The combination of the shortening of the O-H bond-length and increase of the libration's path length and greater deviations from circularity may result in the extremely small (and slightly negative) dependence of the libration frequency under pressure.

1.4.4 Cation bonding environment:

As pressure is increased to the 10-20 GPa range, the Raman spectra show shifts in the relative intensities of several bands in the lattice and cation regions, and one of the pre-existing peaks (with an ambient pressure frequency of 396 cm^{-1}) develops a new shoulder in this region as well (Figure 1.6a-b). Correlation of the

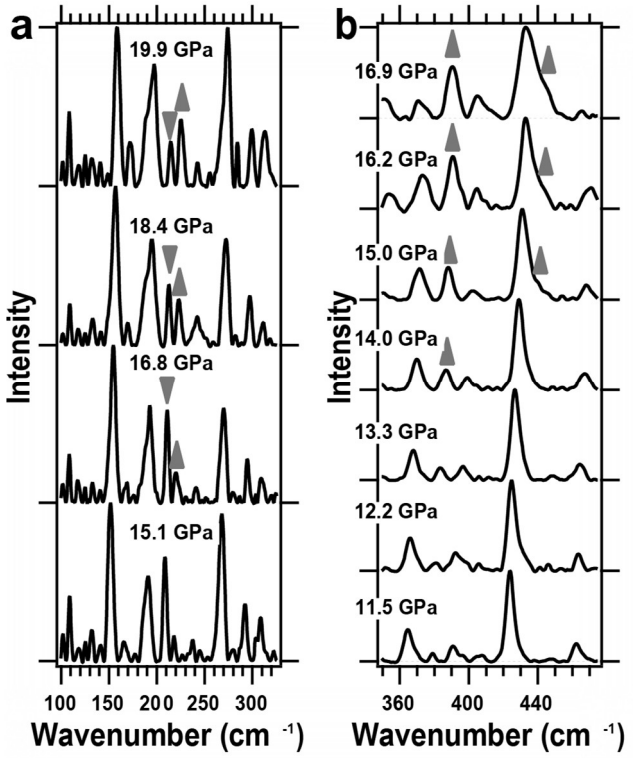

Figure 1.6: Intensity changes in the tremolite Raman spectroscopic peaks of **a)** the lattice modes from 15-20 GPa and **b)** the cation translation modes from 11-17 GPa

assignments of these bands with the theoretical atomic displacements calculated by Caracas and Bobocioiu (2011) indicate extensive involvement of the Ca cation in these vibrations, and thus these intensity variations indicate that there may be changes in the bonding environment of the M4 site in this pressure range. Furthermore, at

pressures beyond 20 GPa, the Raman mode shifts in the range of the cation vibrations display increasingly complex behavior (Figure 1.2)—this may include suggestions of Fermi resonance between neighboring bands (occurring near ~24 GPa and 450 cm^{-1}) and possible peak splitting (near ~26 GPa and 400 cm^{-1}) in the neon-loaded sample. The presence of Fermi resonance between subsets of closely-juxtaposed bands under pressure in tremolite would be unsurprising, as tremolite is expected to display 61 Raman active vibrations with only two symmetry types.

Fluorescence in the sample becomes especially strong in the 20-30 GPa pressure range, where it masks some of the lower-intensity peaks in the region of the spectra dominated by cation vibrations. It is, therefore, difficult to correlate the peak shifts in the cation region with the highest pressures explored in this study, but the complexity of the behavior of the cation bands above 15 GPa is strongly indicative of changes in the bonding environment of the M-sites, especially the M4 site. The high-pressure structural refinements of Comodi et al. (1991) indicated a tendency toward elongation of the flattened bipyramidal octahedral M1, M2, and M3 sites, and homogenization of the Ca-O bond lengths of the M4 sites under compression to 3.5 GPa. With no clear evidence that tremolite undergoes a phase transition in the pressure range of this study, the observed relative intensity changes and complexity observed in the Raman spectra of tremolite are likely indicators of ongoing accommodation of compaction by further distortion of the bonding environment of the M sites (Comodi et al. 1991).

1.4.5 Mode-Grüneisen parameters:

The response of the Raman band frequencies to changes in pressure and temperature is quantifiable by calculation of the mode-Grüneisen parameters. The pressure dependence of the vibrational frequencies of tremolite can be determined by use of the high-pressure Raman spectroscopy to calculate the isothermal mode-Grüneisen parameter, defined as

$$\gamma_{iT} = \frac{K_T}{\omega_{0_i}} \left(\frac{\partial \omega_i}{\partial P}\right)_T \quad (1)$$

where γ_{iT} is the isothermal mode-Grüneisen parameter of the *i*-th vibrational mode, K_T is the isothermal bulk modulus, ω_{0_i} is the frequency of the *i*-th mode at ambient pressure as determined from the ambient pressure intercepts of the Raman mode shifts with the *y*-axis (Figure 1.2), and $(\partial \omega_i / \partial P)_T$ is the slope of the *i*-th mode shift calculated at ambient pressure (Table 1.1). For K_T, we use a value of 85 GPa, as reported by Comodi et al. (1991). The calculated isothermal mode-Grüneisen parameters for both the external modes (the lattice and cation modes) and the internal modes and hydroxyl libration and stretching modes are shown in Figure 1.7a. The external modes are observed to have substantially larger Grüneisen parameters than the internal and hydroxyl modes: this trend is in complete accord with the long-standing observation that lattice/external modes are substantially more dependent on pressure than (typically) higher frequency vibrations that have more of a molecular character. Finally, it is notable that the initial slope in the formulation for the isothermal mode-Grüneisen parameter, $(\partial \omega_i / \partial P)_T$, was modulated by the Me-Eth-

H_2O and Ne pressure-media in their hydrostatic ranges. Therefore, the isothermal mode-Grüneisen parameter, as determined, should be free of non-hydrostatic effects.

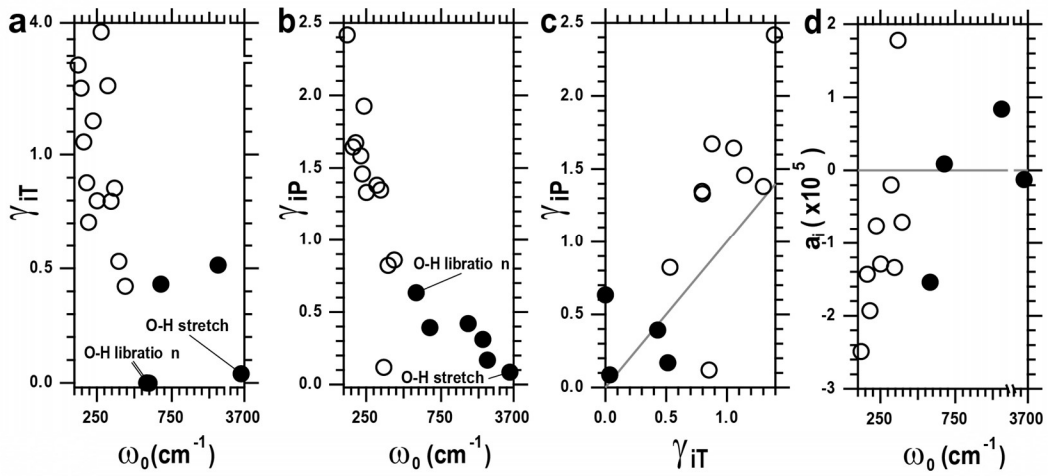

Figure 1.7: **a)** The isothermal mode-Grüneisen parameter and **b)** the isobaric mode-Grüneisen parameter for tremolite. **c)** A comparison plot of the isothermal mode-Grüneisen and isobaric mode-Grüneisen parameters with a zero-anharmonicity reference line. **d)** The intrinsic mode anharmonicity a_i, which removes the volumetric portion of the anharmonicity of the vibrations. Open symbols represent the lattice and cation-involved vibrations; closed symbols represent the internal and hydroxyl-involved vibrations

Similarly, the dependence on temperature can be quantified from the high-temperature data through the isobaric mode-Grüneisen parameter, defined as

$$\gamma_{iP} = -\frac{1}{\alpha\omega_{0_i}}\left(\frac{\partial\omega_i}{\partial T}\right)_P \quad (2)$$

where γ_{iP} is the isobaric mode-Grüneisen parameter of the *i*-th vibrational mode, α is the thermal expansion coefficient, ω_{0_i} is the frequency of the *i*-th mode at room temperature, and $(\partial\omega_i/\partial T)_P$ is the slope of the *i*-th mode shift calculated at room temperature (Table 1.2). We calculate a thermal expansion coefficient (α) value of $2.43 \cdot 10^{-5}\ K^{-1}$ at 294 K using the high-temperature structural parameters of Sueno

et al. (1973) by relating the thermal expansion to volume and temperature at constant pressure as

$$\alpha = \frac{1}{V}\left(\frac{\partial V}{\partial T}\right)_P \quad (3)$$

The isobaric mode-Grüneisen parameters are plotted in Figure 1.7b, illustrating that the external modes also have a stronger temperature dependence relative to the internal and hydroxyl modes.

A comparison of the isothermal and isobaric mode-Grüneisen parameters with a reference line at $\gamma_{iT} = \gamma_{iP}$ illustrates trends in the pressure and temperature dependence of the vibrational modes in tremolite (Figure 1.7c). The internal and hydroxyl modes plot closer to the origin, while the lattice and cation modes plot further away—and generally on the more pressure-sensitive side of the reference line. The $\gamma_{iT} = \gamma_{iP}$ reference line indicates where the shift of the vibrational modes driven by volume changes is equal to zero, and thus modes lying along this line are quasi-harmonic in nature (Gillet et al. 1998). Vibrational modes that plot further from this line show an increasing degree of intrinsic anharmonicity, which is expressed as

$$a_i = \alpha(\gamma_{iT} - \gamma_{iP}). \quad (4)$$

Here, a_i is the intrinsic anharmonicity of the *i*-th mode and $(\gamma_{iT} - \gamma_{iP})$ effectively subtracts out the volumetric portion of the anharmonicity. Our intrinsic anharmonicity results for tremolite indicate that the vibrations associated with the SiO_4 tetrahedra are largely quasi-harmonic—that is, their anharmonicity is primarily volume-independent (Figure 1.7d). The lower frequency vibrations involving the Ca and Mg cations tend to have much more substantial values of intrinsic anharmonicity.

Table 1.1: Isothermal Raman Mode-Shift, Mode-Grüneisen Parameter, and Peak Assignment

ω_0 (cm^{-1})	$d\omega/dP$ (cm^{-1}/GPa)	σ (cm^{-1}/GPa)	γ_{iT}	Assignment
125	2.04	0.06	1.39	lattice mode
145	2.20	0.09	1.29	lattice mode
163	2.02	0.05	1.06	lattice mode
181	1.87	0.07	0.88	lattice mode
195	1.61	0.07	0.71	lattice mode
225	3.04	0.08	1.15	lattice mode
252	2.37	0.10	0.80	lattice mode
278	12.90	14.35	3.96	cation-oxygen translation
323	4.94	0.24	1.30	cation-oxygen translation
345	3.24	0.21	0.80	cation-oxygen translation
368	3.70	0.55	0.85	cation-oxygen translation
396	2.48	0.06	0.53	cation-oxygen translation
439	2.18	0.35	0.42	cation-oxygen translation
582	-0.00	0.04	0.00	hydroxyl libration
599	-0.01	0.06	-0.00	hydroxyl libration
676	3.43	0.09	0.43	ν_1: Si-O-Si symmetric stretch
1059	6.41	0.22	0.51	ν_{as}: Si-O-Si asymmetric stretch
3677	1.73	0.06	0.04	hydroxyl stretch

Table 1.2: Isobaric Raman Mode-Shift, Mode-Grüneisen Parameter, and Peak Assignment

ω_0 (cm^{-1})	$d\omega/dT$ (cm^{-1}/K)*	γ_{iP}	Assignment
125	-0.01	2.42	lattice mode
163	-0.01	1.64	lattice mode
181	-0.01	1.67	lattice mode
218	-0.01	1.58	lattice mode
225	-0.01	1.46	lattice mode
239	-0.01	1.93	lattice mode
252	-0.01	1.33	lattice mode
323	-0.01	1.38	cation-oxygen translation
345	-0.01	1.35	cation-oxygen translation
368	-0.00	0.12	cation-oxygen translation
396	-0.01	0.82	cation-oxygen translation
439	-0.01	0.86	cation-oxygen translation
582	-0.01	0.63	hydroxyl libration
676	-0.01	0.39	ν_1: Si-O-Si symmetric stretch
932	-0.01	0.42	ν_s: O-Si-O asymmetric stretch
1028	-0.01	0.31	ν_{as}: Si-O-Si asymmetric stretch
1059	-0.00	0.17	ν_{as}: Si-O-Si asymmetric stretch
3677	-0.01	0.09	hydroxyl stretch

** All isobaric Raman mode-shifts base on 2-point fits*

The experimental values for the isothermal and isobaric mode-Grüneisen parameters can be compared to the thermodynamic Grüneisen parameter, γ_{th}, defined as

$$\gamma_{th} = \frac{\alpha K_S}{\rho C_P} \tag{5}$$

where K_S is the isentropic bulk modulus, ρ is the density of tremolite, and C_P is the constant-pressure heat capacity. With the assumption that K_S is equal to K_T at 294 K, we can calculate γ_{th} using the values of α and K_T. With 3.05 g/cc as the density of tremolite and a calculated heat capacity of 0.8036 $J/(g \cdot K)$ from the heat-capacity measurements of Krupka et al. (1985), we arrive at a calculated value for γ_{th} of 0.84. This result is in excellent agreement with our Raman-derived average value of 0.89 for the isothermal mode-Grüneisen parameter, while lying below our value of 1.03 for the average of the isobaric mode-Grüneisen parameter. Here, our Raman measurements may somewhat oversample the external modes that tend to have larger Grüneisen parameters (a subset of the highest-lying silicate-associated vibrations tend to be weak in amphiboles), accounting for this modest difference between the vibrational average and the thermodynamic Grüneisen parameter value.

A final interesting aspect of the isothermal mode-Grüneisen parameters is that they decrease markedly at high pressures, as signified by the flattening of the slopes of the pressure-shifts $(\partial\omega_i/\partial P)_T$ (Figure 1.2). There is a substantial curvature in many of the lowest frequency vibrations at low pressures that flatten extensively to have near-zero mode-Grüneisen parameters above 12-15 GPa. This reduction of the

mode-Grüneisen parameters above 10 GPa indicates that low-pressure means of compaction are being saturated. The pressure dependences of the mode-Grüneisen parameters—indicative of a reduction of efficiency of the low-pressure compression mechanisms—imply that the metastable tremolite structure is likely to ultimately become unstable at higher pressures.

1.5 Implications:

The Raman spectra of tremolite display complex behavior of bands associated primarily with cation vibrations beginning at ~15 GPa. However, the lattice modes, internal modes, and hydroxyl stretching modes display normal positive pressure-induced shifts throughout the range of the study, implying that the general topology of the tremolite structure remains metastable to ~50 GPa. The general lack of high-pressure Raman spectroscopic studies of minerals in the amphibole group prevents direct comparisons between the Raman spectra of tremolite and other clinoamphiboles; however, the work of Yang et al. (1998) on the cummingtonite-grunerite solid solution includes high-pressure infrared spectroscopy of the four O-H stretching vibrations of cummingtonite. Yang et al. reported a ~4 cm^{-1} splitting of each of the four hydroxyl bands under compression, occurring in conjunction with the *C2/m-P2₁/m* phase transition in cummingtonite at ~1.29 GPa (1998). There is no resolvable splitting in the tremolite hydroxyl vibrations in the pressure range explored in this study. As the primary difference between tremolite and cummingtonite lies in the occupancy of the M4 crystallographic site (Ca in the former, Mg in the latter), the

M4 site cation may be an important consideration in the metastability of the *C2/m* symmetry structure in tremolite.

Several spectroscopic studies have been carried out exploring the metastability of other inosilicates in the pyroxene and pyroxenoid groups that illustrate notable differences in their high-pressure behavior with regards to tremolite. Serghiou et al. (2000b) observed the pyroxenoids pyroxmangite ($MnSiO_3$) and wollastonite ($CaSiO_3$) to undergo crystalline-amorphous transitions at pressures below 40 GPa, as signified by the disappearance of all Raman modes in the spectra with the exception of a small region of the wollastonite sample (~20 μm) where the presence of a high-pressure crystalline phase was attributed to pressure-gradient effects. Serghiou et al. (2000a, b) reported pressure-induced phase transitions at ~40 GPa for $MgSiO_3$ orthoenstatite and a synthetic $MnSiO_3$ pyroxene (2000b), while the calcic pyroxene diopside ($Ca_{0.5}Mg_{0.5}SiO_3$) transitioned to a high-pressure phase near 55 GPa. Based on changes in the Raman spectra of these pyroxenes in the 700-1200 cm^{-1} region, a change from tetrahedral to octahedral coordination of silicon was proposed as the mechanism for this phase transition, facilitated by polyhedral tilting of the tetrahedral units in the structure (Serghiou et al. 2000a, b). These coordination-change processes in chain silicate minerals are likely to be associated with polyhedral tilting (Jeanloz 1988; Finkelstein et al. 2015; Hu et al. 2017). Hence, the cross-linking of the tetrahedral double-chains in amphiboles may impede the ability of the silica chains to distort into a higher coordination structure, thus extending the metastability range of tremolite to higher pressures than many other inosilicates.

Complex behavior such as the relative intensity shifts of the Raman bands is visible in the spectra of both the Me-Eth-H_2O and the neon loaded samples between 10 GPa and 20 GPa. However, some phenomena such as the possible Fermi resonance and peak splitting near 25 GPa are only visible in the neon data, as many of the cation-related peaks were not resolvable in the Me-Eth-H_2O data due to high fluorescence in the region between 20 GPa and 30 GPa. It is, therefore, difficult to determine whether differences in the Ca-site (M4 site) distortion are present in samples loaded in the two pressure media. With regards to the hydroxyl vibrations, there are subtle differences between the two media, but the shifts of O-H stretching vibration and librations appear largely independent of the non-hydrostaticity of the Me-Eth-H_2O medium at high pressures. Above approximately 35 GPa, there is a subset of the silicate stretching vibrations, cation modes, and lattice modes that undergo substantially smaller pressure shifts in Me-Eth-H_2O than in neon, suggesting that non-hydrostatic effects on the structure impede some types of structural deformation. We speculate that pressure gradients oriented largely along the c-axis in Me-Eth-H_2O may induce internal strains within the crystallites in our experiment that impact tremolite's microstructural response to compression.

The quasi-harmonicity of the SiO_4 tetrahedra, in contrast to the significant intrinsic anharmonicity of the cation vibrations, signifies that the tetrahedral units behave largely rigidly under compaction over the pressure range of this study, while the octahedrally coordinated cations—especially the Ca cations in the M4 sites—undergo significant distortion at higher pressures. At the highest pressures in this

study, the frequencies of the cation-associated, hydroxyl unit, and internal vibrations continue to increase monotonically, while the lattice mode shifts begin to flatten, implying that the compressional mechanisms that affect the lattice vibrations are becoming saturated.

The implications of increased hydrogen localization during the compaction of the tremolite are significant with respect to water-cycling in the deep crust and upper mantle. The relatively small variation under pressure (on a percentage basis) of the O-H vibration implies that D-H partitioning between fluids and amphiboles is probably not notably impacted by pressure (e.g., Graham et al. 1984). Furthermore, the metastability range of tremolite corresponds to depths greater than 1000 km in the Earth and implies that the bulk chemical environment and, at lower subduction-related temperatures, kinetics are of paramount importance in the dewatering and decomposition of tremolite (e.g., Scamburelli et al. 2017). In environments that are likely to metastably preserve tremolite—such as within cold slabs of oceanic crust subducting at a steep angle—tremolite could carry water significantly deeper than the 90 km depth of amphibole breakdown as experimentally constrained at equilibrium conditions. The wide range of tremolite metastability and its potential ramifications for water transport into the deep Earth in subduction zones motivate ongoing investigation of the metastability of tremolite and the monoclinic amphibole structure.

Chapter 2

Metastable Preservation of *C2/m* Tremolite to 40 GPa: A High-Pressure Single-Crystal X-ray Diffraction Study

Jason N. Ott, Bora Kalkan, Genesis Berlanga, Ali F. Yuvali, and Quentin Williams

2.1 Introduction:

The physical and chemical processes that occur at subduction zones are central to understanding the dynamics of the crust and upper mantle of the Earth. The subduction of volatiles, such as the water contained in hydrated mineral phases, is responsible for much of the chemical cycling that occurs in the crust and upper mantle (e.g., Stern, 2002). The dewatering of such phases in the downgoing oceanic lithosphere and accreted sediments leads to flux melting in the overlying mantle wedge and the production of new continental crust through arc volcanism (Pawley and Holloway, 1993). Amphiboles are a complex group of hydrated silicate minerals with a wide range of chemical compositions that form under wide pressure and temperature ranges (Hawthorne, 1981) and therefore are common constituents of altered oceanic crust and metamorphic rocks throughout subduction zones. While the thermodynamic stability of amphiboles has been experimentally constrained to ~2.5 GPa (depths of ~70-90 km) under equilibrium conditions in mid-ocean ridge basalt and andesitic bulk compositions (Poli and Schmidt, 1995; Schmidt and Poli, 1998; Poli and Schmidt, 2002), experimental work has demonstrated that mantle assemblages may potentially contain alkalic amphiboles stable at high temperatures to

pressures extending beyond 12 GPa (e.g., Konzett and Fei, 2000). Furthermore, several studies, including our recent spectroscopic study of the calcic amphibole mineral tremolite, suggest that the metastability of amphibole structures may extend much further—to pressures as high as 50 GPa—in low-temperature/favorable chemical environments (Thompson et al., 2016; Yong et al., 2019; Ott and Williams, 2020).

The amphibole mineral tremolite ($Ca_2Mg_5Si_8O_{22}(OH)_2$) is an inosilicate with monoclinic symmetry that crystallizes in the crystallographic space group *C2/m* (Hawthorne, 1981). Figure 2.1 illustrates the general structure of tremolite and other monoclinic amphiboles—that of an interconnected network of I-beams composed of double-chains of corner-sharing SiO_4 tetrahedra (T1 and T2 crystallographic sites) sandwiching sheets of octahedrally coordinated divalent Mg cations (M1, M2, and M3 sites) extending along the *c-axis* with Ca^{2+} cations (M4 sites) cross-linking the offset stacks of I-beams along the *b*-direction (Papike and Ross, 1970; Law and Whittaker, 1980). Adjacent I-beams along the *a*-direction are separated by the A site in amphiboles, which is vacant in the tremolite structure and is shown in Figure 2.1 as a void in the structure between the Ca cations along the *b*-axis.

The structure of tremolite has been studied previously at ambient conditions by X-ray and neutron diffraction (Hawthorne and Grundy, 1976), at low and high temperatures (Sueno et al., 1973; Yang and Evans 1996), and high-pressure X-ray structural refinements of tremolite were performed to a maximum pressure of 4.1 GPa by Comodi et al. (1991). The previous diffraction studies of tremolite did not observe

any pressure- or temperature-induced phase transitions. However, phase transitions have been found in other monoclinic amphiboles at elevated pressures and

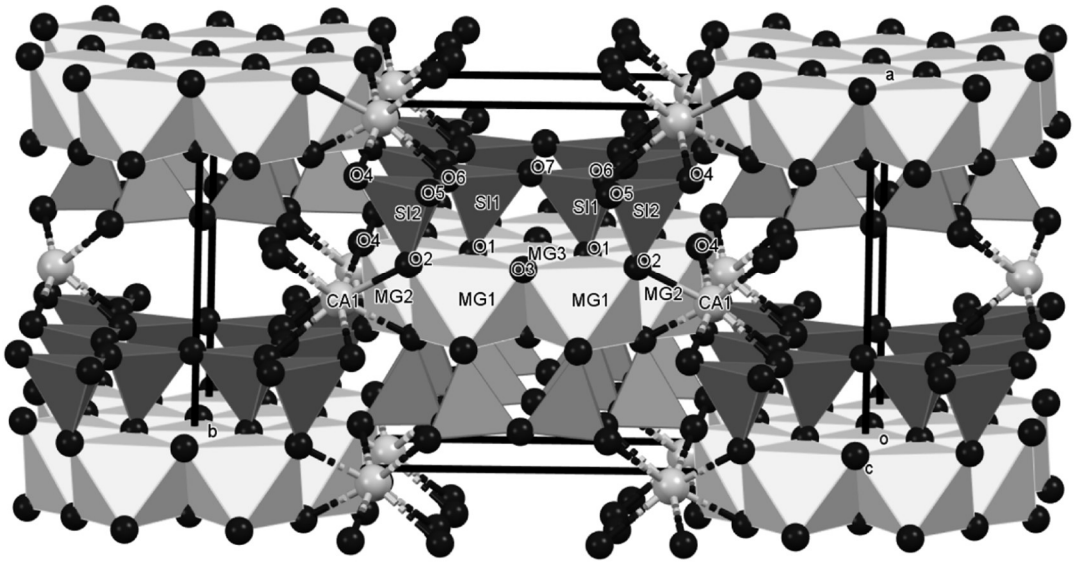

Figure 2.1: Ambient pressure structure of the amphibole mineral tremolite, crystallizing in the C2/m space group. Hydroxyl units, extending from O3 into the cavity in the ring of SiO_4 tetrahedra were not resolved in the XRD data, and are not displayed in the structure

temperatures. In the cummingtonite-grunerite solid solution series ($(Mg,Fe)_2(Mg,Fe)_5Si_8O_{22}(OH)_2$), pressure-induced phased transitions have been observed from the *C2/m* to *$P2_1/m$* space groups at ~1.21 GPa for cummingtonite (Yang et al., 1998) and ~3 GPa for grunerite (Yang et al., 1998; Boffa Ballaran et al., 2000; Yong et al., 2019). A second phase transition was reported for grunerite from the *$P2_1/m$* to *C2/m* space groups at ~19.2 GPa (Yong et al., 2019). A temperature-induced transition in cummingtonite has been observed from the *$P2_1/m$* to the *C2/m* space group in the 240 K to 373 K range, depending upon its composition and cation

site occupancies (Prewitt et al., 1970; Sueno et al., 1972; Yang and Smyth, 1996). The structural similarity between the cummingtonite-grunerite solid solution and tremolite suggests the possibility of similar phase transitions in tremolite. Our Raman spectroscopic study to 49 GPa showed indications of possible shifts in compressional mechanisms at pressures above 10 GPa, but the nature of these shifts in the compression of tremolite is unknown (Ott and Williams, 2020).

In this study, we perform single-crystal X-ray diffraction experiments with synchrotron radiation to investigate the compressibility and metastability of tremolite to ~40 GPa. We refine the structure of tremolite under ambient conditions and determine the unit cell parameters and volume of the tremolite structure under compression at quasi-hydrostatic conditions, and conduct an analysis of the elastic response of the mineral. Our objectives are to determine whether tremolite undergoes any subtle phase transitions or changes in its compressional mechanisms during compaction and to compare the high-pressure behavior of tremolite to that of other monoclinic amphiboles under pressures relevant to the crust and upper mantle in subduction zones.

2.2 Experimental Methods:

The tremolite used in this study is a natural sample, sourced from the Crevoladossola marble of the Novara province of Italy. We performed a Raman spectroscopic study of crystals from the same bulk sample previously, and there were no indications of calcite or dolomite inclusions in the mineral. There is also no

evidence of significant substitution of Fe^{2+} for Mg^{2+} in the M1, M2, or M3 octahedral sites, and therefore the mineral appears to be of nearly end-member composition (Ott and Williams, 2020).

Ambient and high-pressure single-crystal X-ray diffraction studies were carried out at beamline 12.2.2 at the Advanced Light Source (ALS), Lawrence Berkeley National Laboratory. Elongated crystals from the tremolite hand sample were crushed in an agate mortar and pestle, and several block-shaped single-crystals with no visible fractures were selected for this study.

2.2.1 Ambient Conditions X-ray Diffraction:

An irregularly shaped tremolite single-crystal was selected under a polarized microscope using a micromesh mount (Mitegen USA) with 30 μm aperture size, and was mounted on the goniometer of the STOE StadiVari X-ray single-crystal diffractometer at end-station 1 of beamline 12.2.2. The diffraction data were collected with an RDI CMOS 1M detector. Shutterless single-crystal X-ray diffraction measurements were performed using synchrotron radiation monochromated by silicon (111) at an energy of 30 keV (0.4133 Å). Data collection (ϕ-scans) was performed at room temperature at step widths of 1° using an x-ray beam focused to ~ 20 μm. A typical exposure time of 0.5-2 s/° that maximizes the intensities of the diffraction peaks without saturation was selected. A NIST standard (SRM 1990, single-crystal ruby sphere) was used to calibrate the beamline characteristics, such as sample distance and wavelength (Wong-Ng et al., 2001). Data were integrated using XAREA

1.76 (Stoe and Cie, 2009). Integrated intensities were scaled and corrected for absorption (with the numerical absorption correction) using LANA (Koziskova et al., 2016) and X-RED32 (equivalent to the work of Coppens (1970)) packages embedded in XAREA. Structures were solved using direct methods in SHELXS and further refined anisotropically using SHELXL (Sheldrick, 2008).

2.2.2 High-Pressure X-ray Diffraction:

High-pressure diffraction data were collected using tremolite single-crystals of dimensions ~10 x 20 x 20 μm loaded into either a BX-90 diamond anvil cell (DAC) equipped with 350 μm culet type Ia diamond anvils, or a short symmetric-type DAC equipped with 300 μm culet 80° aperture Boehler-Almax type diamonds. The gaskets were machined by pre-indenting 250 μm thick rhenium to 30 μm thickness, and a circular 130 μm diameter sample chamber was drilled with a laser-milling system. Residue from the laser milling process was removed by hand initially, and then gaskets were cleaned ultrasonically with acetone followed by deionized water. Gaskets were mounted to the piston-side diamond anvil, and the tremolite crystals loaded at the center of the sample chamber and several small ruby crystals (< 10 μm diameter) placed around the sample as a pressure standard. The DAC was gas loaded at the ALS with neon gas as a pressure transmission medium, as this medium has been shown to behave close-to-hydrostatically up to pressures approaching 50 GPa (Klotz et al., 2009). Diffraction data were collected up to ~47 GPa over pressure-steps ranging from 0.5 to 5 GPa. After sample equilibration with each pressure-step,

pressure measurements were made using ruby fluorescence in conjunction with the R1 and R2 peak locations (Mao et al., 1986). Pressure measurements were repeated after collection of each set of diffraction images to monitor for any drift in pressure.

The high-pressure diffraction data were collected at end-station 2 of beamline 12.2.2 using synchrotron X-rays monochromated by silicon (111) with an energy of 25 keV (wavelength of 0.4959(1) Å) that was focused to a 10 x 10 μm spot. The beam was passed through a Pd/Sn filter upstream of the DAC, and diffracted X-rays were collected on a Perkin-Elmer amorphous silicon detector covered in 5 layers of 24 μm thick Al foil to reduce the intensity and facilitate unsaturated 2-second exposure times at each increment. Detector distance and wavelength calibration were performed using a NIST single-crystal ruby sphere (Wong-Ng et al., 2001). The sample was aligned to the rotational center of the goniometer, and data collected throughout the range of $\theta = -35°$ to $35°$ (in $0.25°$ and $0.10°$ increments) for a total coverage of $70°$ sample rotation.

Data collection was performed using a LabView code produced at the ALS, and data were analyzed using APEX3 (Bruker, 2016). Unit cell parameters at each pressure-step were determined up to 38.7 GPa by a least-squares refinement of ~300 reflections harvested from 200 frames in the $\theta = -35°$ to $+35°$ range. After indexing of the diffraction pattern and determination of the Bravais lattice, the NIST ruby calibration was applied, and the unit cell parameters were refined. Loss of intensity in the diffraction data collected at pressures above 38.7 GPa resulted in a weak

peak/background ratio in the reciprocal lattice that prevented indexing and refinement of the unit cell parameters.

2.3 Results and Discussion:

2.3.1 Ambient Pressure Structural Refinement and Unit Cell Parameters:

Analysis of the ambient pressure single-crystal data produced a structure for tremolite with unit cell parameters a = 9.833(2) Å, b = 18.0459(36) Å, c = 5.2736(11) Å, β = 104.756(30)°, and V = 904.89(30) Å^3 and symmetry consistent with the *C2/m* space group. The atomic positions of the ambient pressure structural refinement are presented in Table 2.1 and Figure 2.1. This result is in excellent agreement with previous work on near end-member composition tremolite at ambient conditions (e.g., Comodi et al., 1991; Yang and Evans, 1996). In particular, the β-angle, which is sensitive to small amounts of cummingtonite substitution (Yang and Evans, 1996), is indistinguishable from tremolites with negligible substitution. Atomic positions from our ambient pressure structural refinement were used to calculate the thickness and separation of the I-beam structural unit. Our measured thickness of 6.59 Å at the center of the I-beam (O7-O7' distance) and 7.05 Å at the edge (O4-O4' distance) are respectively 2.6 and 1.4% larger than the room-pressure results of Comodi et al. (1991). Still, we find a similar value for the reduction in thickness at the center of the I-beam (~.5 Å) attributable to the bowed structure of the SiO_4 double-chains in amphiboles as reported in previous studies (e.g., Papike and Clark, 1968; Comodi et al., 1991). The hydrogen atoms were not resolvable in the electron density map and,

Table 2.1: Atomic coordinates and the anisotropically refined displacement parameters for the tremolite structure (monoclinic *C2/m* space group) at ambient conditions.

Atom	x	y	z	U_{eq}
Mg1	0	0.08801(10)	0.5	0.00550(41)
Mg2	0	0.17639(10)	0	0.00510(41)
Mg3	0	0	0	0.00480(52)
Ca1	0	0.27794	0.5	0.00850(31)
Si1	0.28089(9)	0.08394(6)	0.29759(19)	0.00465(30)
Si2	0.28862(8)	0.17114(6)	0.80554(19)	0.00421(29)
O1	0.11209(22)	0.08552(14)	0.21820(50)	0.00603(60)
O2	0.11879(22)	0.17053(15)	0.72409(49)	0.00605(58)
O3	0.10640(30)	0	0.71439(66)	0.00369(74)
O4	0.36501(22)	0.24808(16)	0.79246(49)	0.00700(59)
O5	0.34655(22)	0.13447(16)	0.10005(48)	0.00648(57)
O6	0.34457(22)	0.11891(15)	0.58960(50)	0.00645(57)
O7	0.33867(32)	0	0.29327(75)	0.00768(80)
Measured reflections			3421	
Independent reflections			845	
Parameters refined			97	
R_{int}			0.0969	
Goodness of fit			1.080	
wR_2			0.1015	
R_1 (all 845 data)			0.0528	
R_1 (677 data Fo > 4 σ_{Fo})			0.0382	

therefore, were not included in the refinement of the tremolite structure. Results for the unit cell parameters and volume of the tremolite structure for the ambient and high-pressure experiments are presented in Table 2.2, and the normalized change in the volume and unit cell parameters are shown to 38.7 GPa in Figure 2.2. Tremolite persists in the *C2/m* space group throughout the pressure range investigated, with no apparent discontinuities in the volume or axial parameters, and thus no indication that tremolite undergoes a first-order phase transition over the pressure range of this study, in accordance with our Raman results (Ott and Williams, 2020).

Table 2.2: Unit cell parameters and volumes of tremolite at pressures up to 38.7 GPa. Tremolite structure symmetry is *C2/m* for all pressures investigated. Set 0 is the ambient conditions dataset, Sets 1 and 2 are high-pressure DAC measurements in a Ne gas transmission medium.

Set	Pressure (GPa)	a (Å)	b (Å)	c (Å)	β (°)	V (Å^3)
0	0.0001	9.833(2)	18.0459(36)	5.2736(11)	104.756(30)	904.9(3)
1	1.0	9.751(7)	17.9836(10)	5.2613(3)	104.923(20)	891.5(7)
2	1.9	9.707(2)	17.9663(13)	5.2485(3)	104.949(8)	884.4(2)
1	2.5	9.675(8)	17.9115(12)	5.2423(4)	105.210(20)	876.7(7)
1	3.7	9.598(6)	17.8530(8)	5.2253(2)	105.183(17)	864.1(5)
1	4.9	9.558(4)	17.7960(11)	5.2106(3)	105.276(13)	854.9(4)
2	5.9	9.519(2)	17.7856(13)	5.2010(3)	105.185(9)	849.8(2)
1	7.2	9.476(4)	17.6935(10)	5.1863(3)	105.397(13)	838.3(3)
1	8.8	9.423(4)	17.6235(11)	5.1690(3)	105.455(14)	827.4(4)
2	9.4	9.407(2)	17.6438(14)	5.1681(3)	105.284(9)	827.4(2)
2	10.0	9.392(3)	17.6175(15)	5.1618(3)	105.287(9)	823.9(2)
1	10.3	9.383(4)	17.5682(10)	5.1548(3)	105.469(13)	818.9(3)
1	11.1	9.335(4)	17.5408(10)	5.1489(3)	105.485(13)	812.5(4)
2	11.6	9.334(2)	17.5575(14)	5.1483(3)	105.272(9)	813.9(2)
1	12.0	9.305(3)	17.5050(9)	5.1402(2)	105.523(11)	806.7(3)
1	12.9	9.289(4)	17.4767(10)	5.1332(3)	105.525(12)	803.0(3)
2	13.9	9.268(2)	17.4762(14)	5.1305(3)	105.274(9)	801.6(2)
1	14.3	9.245(4)	17.4204(10)	5.1190(3)	105.499(12)	794.4(3)
2	14.8	9.233(2)	17.4362(14)	5.1217(3)	105.247(9)	795.5(2)
1	15.3	9.228(4)	17.3850(10)	5.1133(3)	105.476(12)	790.6(3)
1	16.2	9.202(4)	17.3576(11)	5.1049(3)	105.454(14)	785.9(3)
1	17.4	9.170(5)	17.3214(12)	5.0983(3)	105.388(15)	780.8(4)
2	22.1	9.040(3)	17.1989(16)	5.0800(3)	105.119(11)	762.5(2)
2	24.5	8.994(3)	17.1392(18)	5.0696(3)	105.153(11)	754.3(2)
2	28.0	8.920(4)	17.0400(30)	5.0555(5)	105.000(17)	742.2(3)
2	31.3	8.894(5)	17.0140(30)	5.0460(5)	105.192(16)	736.9(3)
2	33.1	8.870(5)	16.9630(30)	5.0404(5)	105.217(18)	731.8(4)
2	35.8	8.846(7)	16.9510(40)	5.0334(7)	105.310(20)	727.9(5)
2	38.7	8.749(8)	16.8430(50)	5.0211(7)	105.130(20)	714.3(6)

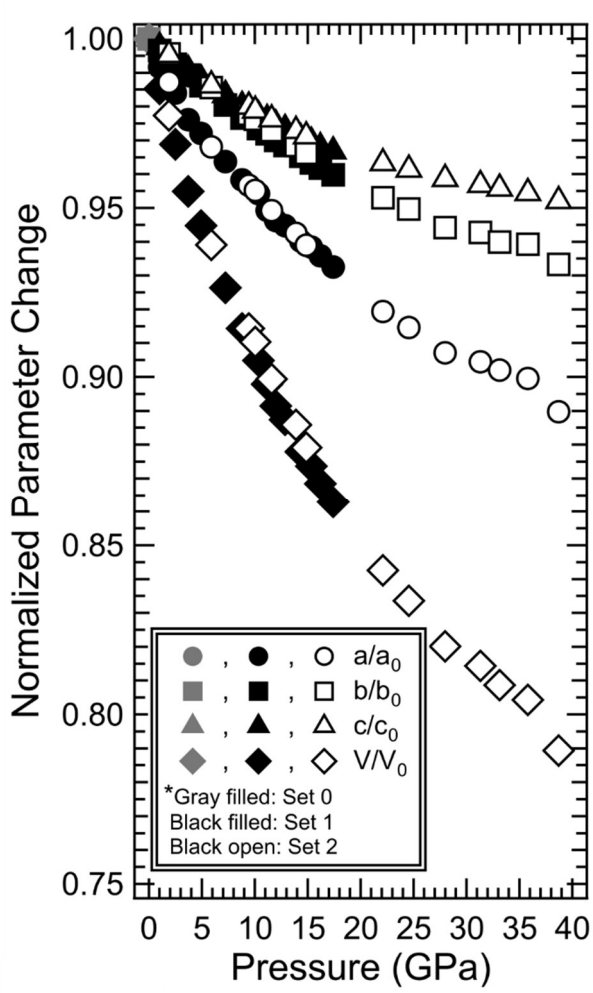

Figure 2.2: The normalized unit cell parameters (a/a_0, b/b_0, and c/c_0) and the normalized volume (V/V_0) of tremolite to ~39 GPa. Set 0 at ambient conditions, Sets 1 and 2 at high pressures in DAC with Ne pressure-medium. Uncertainties of the parameters are contained within the markers

The evolution of the monoclinic β-angle in tremolite over the pressure range of the experiment is, however, complex. Figure 2.3 shows the change in the β-angle as a function of pressure, which initially increases, as in other monoclinic amphiboles investigated by high-pressure single-crystal XRD studies (Comodi et al., 1991; Yang et al., 1998; Yong et al., 2019). However, in tremolite, the β-angle reaches a

maximum between 10 and 13 GPa and begins decreasing, until ~22 GPa, where the trend reverses, and the β-angle again weakly increases. As the data collected above 38.7 GPa could not be indexed, it is unclear whether the decrease in the β-angle at the maximum pressure datum represents another change in the trajectory of the β-angle or scatter/uncertainty in the data.

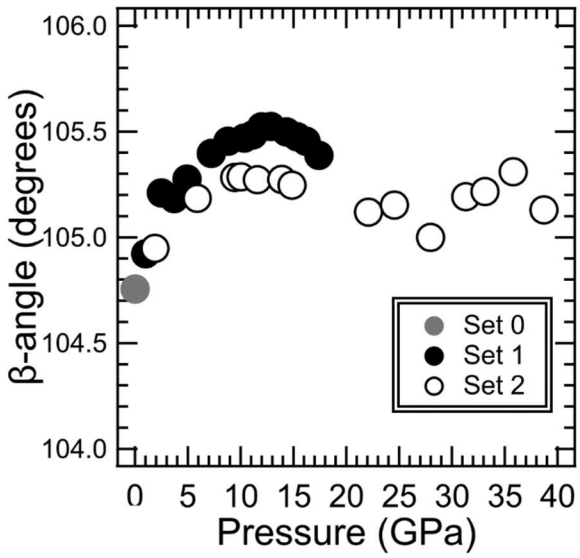

Figure 2.3: Response of the β-angle of C2/m monoclinic space-group member tremolite to high pressures in Ne pressure-transmission medium loaded DAC. Uncertainties are contained within the markers

Whittaker (1960) ties the M4-O4 bond length and the radius of the ion occupying the M4 site to the β-angle of monoclinic amphiboles, which in turn can be related to the degree of closest packing of the oxygen anions in the structure (Yang et al., 2019). In the X-ray diffraction studies by Yang et al. (1998) on cummingtonite and Yong et al. (2019) on grunerite, the M4 site is primarily occupied by Fe^{2+} cations and the initial β-angle of ~102° increases through the entire pressure range of their experiments. Yang et al. (1998) and Yong et al. (2019) observe that during the *C2/m*-

P2₁/m phase transition the SiO_4 double chain becomes two distinct chains: an O-rotated B-chain corresponding to the sense of rotation of both chains in the *C2/m* structure, and an S-rotated A-chain (Papike and Ross (1970) provide a discussion of chain rotation in inosilicates). This reduction in symmetry of the structure is accompanied by an increase in the coordination of the M4 sites in cummingtonite and grunerite from six—two M4-O2 bonds, two M4-O4 bonds, and two M4-O6 bonds—to seven by the inclusion of one M4-O5 bond in the coordination of the M4 site. The *P2₁/m-C2/m* phase transition to γ-grunerite at ~19 GPa described by Yang et al. (2019) notes a return of both tetrahedral chains to an O-rotated configuration in conjunction with a discontinuous increase in the *β*-angle to 107.99° and a return of the M4 site to six-fold coordination—with the difference that the M4 site is now coordinated to two O5 anions in place of the two O6 anions in the low-pressure *C2/m* phase. Therefore, the sequence of increasing-pressure phase transitions in the cummingtonite-grunerite solid solution allows the oxygen anions to move into more closely packed configurations with higher pressures. In contrast, the M4 site of tremolite, with its larger, eight-fold coordinated Ca^{2+} cations, generates a larger ambient pressure *β*-angle, implying that the oxygen anions are more closely packed than in the cummingtonite-grunerite solid solution series at low pressures. Indeed, the ambient pressure volume of tremolite is ~1% less than that of grunerite (Yong et al., 2019). The increase of the *β*-angle to a maximum at pressures of ~10-13 GPa, followed by a decreasing trend that reverses to weakly increase at pressures greater than 22 GPa, suggests that the structural accommodation of compression in tremolite

is governed by steric effects created by the presence of the more sizeable calcium cation in the M4 site of tremolite and its coordination to eight oxygen anions throughout its compaction.

2.3.2 Bulk Moduli, Equations of State, and Axial Compressibilities:

While our analysis shows that tremolite does not undergo a phase transition up to 39 GPa, there are, nonetheless, small slope changes in the trends of the axial parameters and the volume of the tremolite unit cell with increasing pressure. These slope changes are clearly apparent in the variations of the axial ratios of the unit cell with pressure. Figure 2.4 illustrates the axial ratios *a/b* and *a/c* for tremolite alongside the ratios reported for cummingtonite (Yang et al., 1998) and grunerite (Yong et al., 2019). The reported results of Yang et al. (1998) display a change in the slopes of *a/b* and *a/c* that occurs in conjunction with the *C2/m-P2$_1$/m* phase transition in cummingtonite. Interestingly, in the results of Yong et al. (2019), the axial ratios for grunerite show slope changes and discontinuities that occur with the *C2/m-P2$_1$/m* transition near ~7 GPa and the *P2$_1$/m-C2/m* transition near ~19 GPa. Both the studies of cummingtonite and grunerite conclude that changes in compression mechanisms occurred in conjunction with the observed phase transitions. The axial ratios for tremolite suggest that the structure also undergoes changes in its compressional mechanisms, with the first change being near ~5 GPa and a second near ~22 GPa. Notably, the apparent changes in the compression mechanism of tremolite occur at

close to the same pressures as the phase transitions and compressibility changes observed in grunerite.

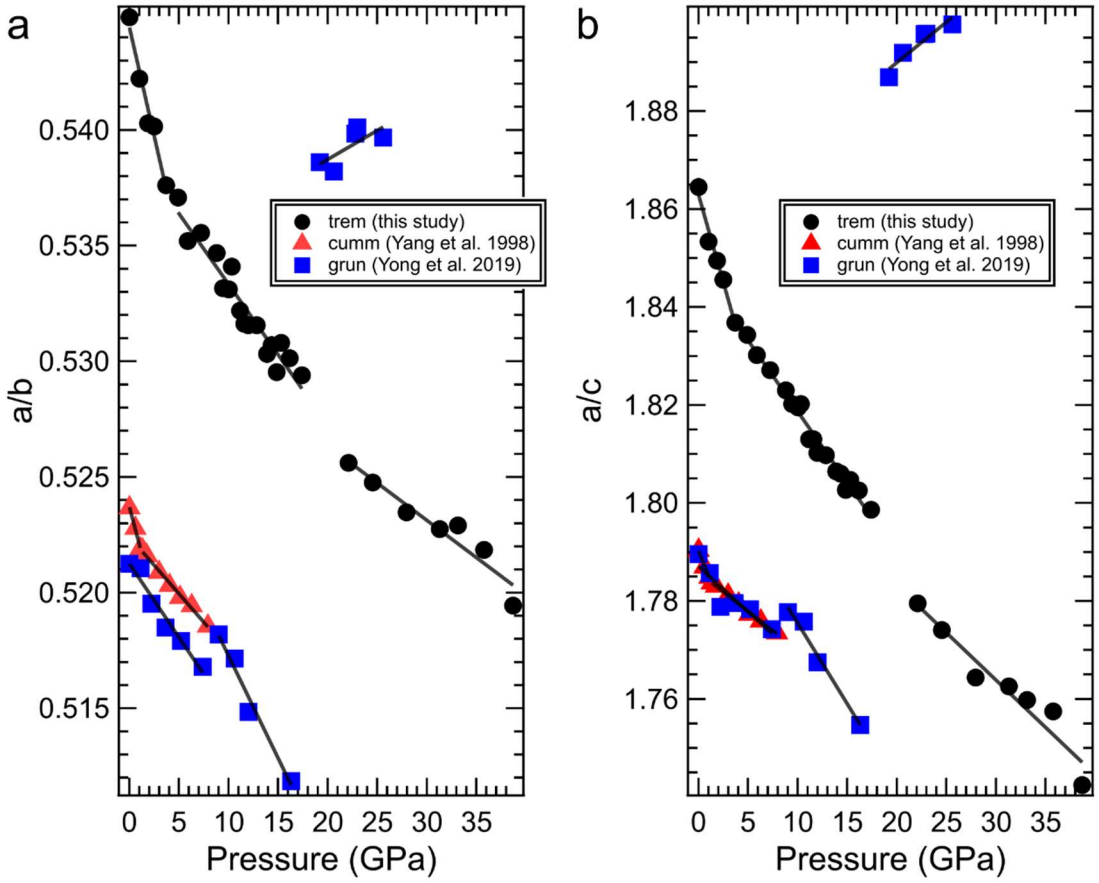

Figure 2.4: Unit cell parameter ratios **a)** a/b and **b)** a/c for the monoclinic amphiboles tremolite with increasing pressure. Plots of the ratios for cummingtonite (Yang et al., 1998), and grunerite (Yong et al., 2019) included for comparison. Slopes of the axial ratios for each region are fit by method of least squares

In fitting the pressure and volume data to an equation of state, data were transformed and plotted on an F_E-f_E plot, where f_E was calculated using the Eulerian definition of finite strain as

$$f_E = \frac{1}{2}\left[\left(\frac{V_0}{V}\right)^{2/3} - 1\right] \quad (1)$$

and F_E is the normalized pressure determined as

$$F_E = \frac{P}{3f_E(1+2f_E)^{5/2}} \quad (2)$$

using the methodology described by Birch (1978). The F_E-f_E plot for our tremolite data is presented in Figure 2.5a and suggests that there are three separate regimes of compressional behavior, which we refer to as, with increasing pressure, tremolite compression regimes I, II, and III. The slope changes occur at finite strains

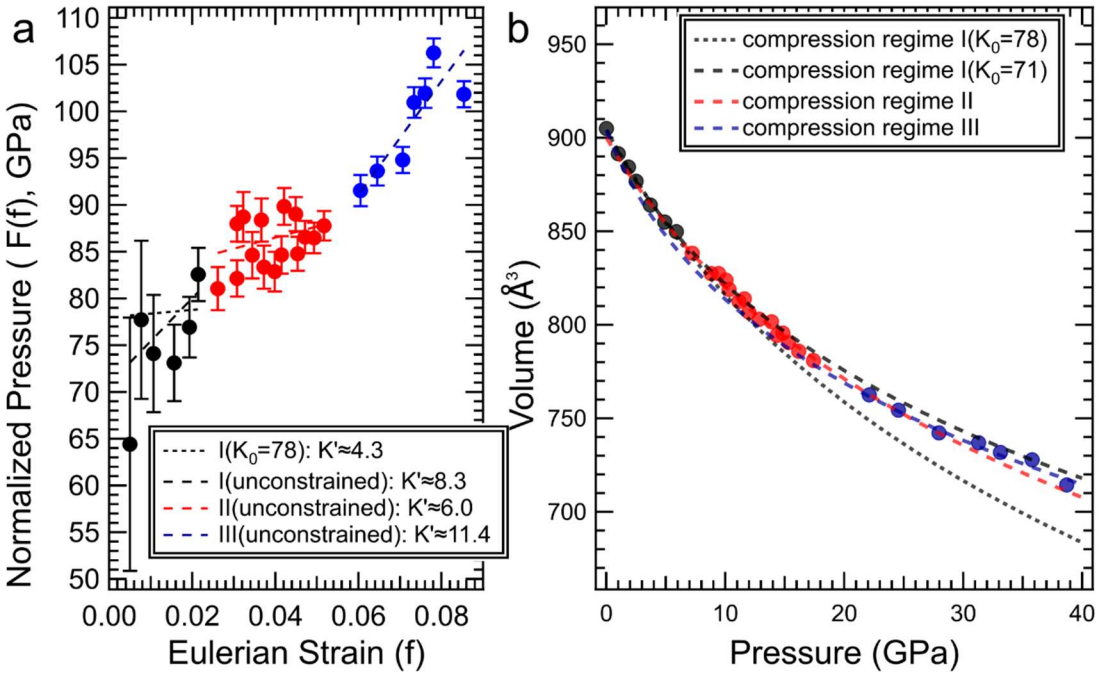

Figure 2.5: **a)** F_E-f_E plot for tremolite with least squares fit lines for the determination of K_{0T} and K'_{0T} for each compression regime and **b)** the unit cell volumes of tremolite plotted with fits of a third-order Birch-Murnaghan equation of state

corresponding to ~5 GPa and ~22 GPa, which is consistent with the changes in the slopes of the axial ratios of tremolite (Figure 2.4). The relationship with the changes in the β-angle is less clear, but the higher-pressure shift may be associated with a

change in the pressure-dependence of this angle. Least-square fit trendlines to the F_E-f_E data display linear trends with *increasingly* positive slopes in each regime and thus indicate that the data are best described using a sequence of third-order equations of state (Angel, 2000b). The values of K_0 and K' can then be estimated by applying the equations:

$$F_E = K_0(1 + a\,f) \qquad (3)$$

with K_0 determined as the intercept of the fit line with the F_E-axis (Figure 2.5a), and

$$K' = \frac{2}{3}a + 4 \qquad (4)$$

for data fit by a third-order equation of state (Birch, 1978; Angel, 2000b). Data in compression regime I were also fit using a constrained isothermal bulk modulus of 78 GPa as determined for tremolite by Brown and Abramson (2016) using Reuss bounds and elastic moduli measured by impulsive stimulated light scattering. The volume and pressure data for each compression regime were used along with our estimated values for K_0 and K' to fit third-order Birch-Murnaghan equations of state with the program EosFit7:GUI (Gonzalez Platas et al., 2016), and the results are shown in Figure 2.5b and Table 2.3. Our unconstrained third-order fit of the equation of state of tremolite in compression regime I results in a significantly lower value of K_0 (71 (±8) GPa) than the value of 85 GPa reported by Comodi et al. (1991). The disagreement can be attributed to our use of a third-order finite strain equation of state relative to their linear fit of pressure-volume data (which implicitly assumes a K' of 0). The value of K_0 of tremolite was reanalyzed by Comodi et al. (2010) using a second-order equation of state (an assumed K' of 4) using the Comodi et al. (1991) data, resulting

in a K_0 of 76 (±3). The values of K' that we generate (8.3 (±2.9) for our unconstrained third-order fit, and 4.3 (±0.8) for the fit with the bulk modulus constrained) would bring these values into better agreement. Values of K' that are greater than 4 for tremolite are also indicated by first-principles calculations (Peng and Mookherjee, 2020): these yield, with the local density approximation, a bulk modulus of 78.5 GPa, a K' of 5.2, and a zero pressure volume underestimated by 2%.

Table 2.3: Third-order Birch-Murnaghan equation of state data for tremolite

Compression Regime	I	I*	II	III
P_{min} (GPa)	0.0001	0.0001	7.2	22.1
P_{max} (GPa)	5.9	5.9	17.4	38.7
K_{0T} (GPa)	71(8)	78*	82(3)	55(1)
K'_{0T}	8.3(29)	4.3(8)	6.0(1)	11.4(1)
V_0	904.37(90)	904.25(70)	900.06(55)	904.11(69)
β_a	0.0082(4)		0.0053(17)	0.0029(10)
β_b	0.0037(19)		0.0025(8)	0.0028(4)
β_c	0.0029(2)		0.0024(13)	0.0021(1)
$\beta_a:\beta_b:\beta_c$	2.22:1.0:0.78		2.12:1.0:0.96	1.03:1.0:0.75

*Constrained fit with a fixed bulk modulus of 78 GPa

Tremolite compresses anisotropically over the pressure range explored in the experiment, with the greatest reduction of unit cell length occurring along the *a*-axis (~11% reduction at 38.7 GPa), followed by the *b*-axis (~7% reduction), and the least compressible direction along the *c*-axis (~5% reduction). The axial compressibilities of tremolite, defined by Angel (2000a) as $\beta_{10} = 1/(3K_{10})$, were calculated using the program EosFit7:GUI (Gonzalez Platas et al., 2016) to fit the third-order Birch-

Murnaghan equation of state to the unit cell parameter data for each compression regime (Table 2.3). Tremolite's initial compressibilities β_a, β_b, and β_c are calculated as 0.0082(4), 0.0037(19), and 0.0029(2) GPa^{-1}, respectively. Our results for β_b and β_c agree within the estimated standard deviations to the values of $\beta_b = 0.0027$ GPa^{-1} and $\beta_c = 0.0026$ GPa^{-1} reported by Comodi et al. (1991), while our higher result of β_a=0.0082 GPa^{-1} (reported as 0.0059 GPa^{-1} by Comodi et al.) again stems from the difference between a linear pressure-axial length fit as opposed to a third-order equation of state (as in our calculations), which allows for refinement of the pressure-derivative of the compressibility.

Another notable difference between tremolite and the amphiboles of the cummingtonite-grunerite solid solution becomes apparent in a comparison between axial compressibilities. In our analysis of tremolite, we calculate the initial axial compression ratio (β_a:β_b:β_c) as 2.22:1.0:0.78, while Yang et al. (1988) reported 2.83:1.00:1.17 for the low-pressure *C2/m* phase of cummingtonite and Yong et al. (2019) calculated a ratio of 1.49:1.00:1.10 for *C2/m* α-grunerite. All three minerals are highly anisotropic under compaction, with the *a*-axis being the most compressible direction. However, for tremolite, the *c*-axis is the least compressible direction, while for cummingtonite and grunerite, it is the *b*-axis. Since the changes in the compressibility for grunerite occur with phase transitions at similar pressures to the compressibility changes in tremolite, it is interesting to contrast the behavior of the two minerals across the three compression regimes we observe in tremolite, and the transitions in grunerite. With each change in the compression mechanism of

tremolite, the compressibilities along the *a*- and *c*-axes are reduced, while along the *b*-axis, the compressibility fluctuates near ~.0030 GPa^{-1} (Table 2.3) leading to a general reduction in the compressional anisotropy of tremolite with each regime change. In contrast, as grunerite transitions from *C2/m* α-grunerite → *P2₁/m* β-grunerite → *C2/m* γ-grunerite, the ratios $\beta_a : \beta_b : \beta_c$ evolve from 1.49:1.0:1.1 → 1.86:1.0:0.99 → 0.56:1.00:1.41 with the compressibility along the *b*-axis again fluctuating in a narrow region, and increasingly anisotropic compressibility along the other crystallographic axes (Yong et al., 2019). Hence, the compressional anisotropy of tremolite is substantially decreased by pressure, with the relative ratios of axial compressibilities being 1.03:1.0:0.75 in the highest-pressure compressional range. A decrease in anisotropy of tremolite under compression is also observed in theoretical results (Peng and Mookherjee, 2020), but the evolution towards nearly equal compressibilities of the *a* and *b* axes involves a substantially more isotropic compressibility than is observed in the theoretical results. In contrast, the compressional anisotropy of grunerite is augmented by its sequence of transitions. Thus, the substantial stiffening of the *a*-axis in tremolite under compression implies that the vacant A-site and the octahedral layers become substantially less compressible at the highest pressures of this study.

The compression mechanism of tremolite in compression regime I (<6 GPa) has been characterized in the work of Comodi et al. (1991) and consists largely of a flattening of the bowed tetrahedral chains along the *b*-axis and, consequently, a reduction in the volume of the vacant A-site of the structure. Compaction along the

less compressible *b*- and *c*-axes is primarily accommodated by an increased sense of O-rotation in the SiO_4 tetrahedral double-chains and distortion of the M site polyhedra. The compressional mechanisms acting in regimes II and III are consistent with the presence of eight-fold coordinated calcium cations in the M4 site being critical in the inhibition of transitions into more closely packed structures and, thus, the calcium cations are also likely to be a significant factor in determining the avenues of compression available to tremolite in compression regimes II and III. This importance of the M4 site in the compressional behavior of tremolite is supported by the results of our previous Raman spectroscopic study of tremolite to ~50 GPa, in which the appearance of spectral features above 10 GPa are indicative of changes in the bonding environment of the M4 site, but again with no evidence that tremolite undergoes a phase transition (Ott and Williams, 2020).

2.4 Implications:

Structural similarities between single- and double-chain inosilicates naturally lead to comparisons of the structural properties and phase transition behavior of the pyroxene and amphibole structures. The sensitivity of phase transitions to M site cation size and shifts in M site coordination through a sequence of $C2/c$-$P2_1/c$-$C2/c$ phase transitions in high-pressure studies of both natural and synthetic clinopyroxenes has been previously noted (e.g., Arlt et al., 1998; Arlt and Angel, 2000; Yang and Prewitt, 2000; Tribaudino et al., 2001), although high-pressure structural studies of the clinoamphiboles have been limited. The cummingtonite-grunerite solid solution

series undergoes a series of potentially analogous phase transitions at 300 K in clinoamphiboles under compression, but the preservation of the *C2/m* phase of tremolite to pressures of 40 GPa and higher raises questions of the role that calcium plays in dictating the high-pressure metastability of tremolite. A plausible explanation for this difference in behavior is that the size and occupancy of the eight-fold Ca cation site in tremolite impedes the ability of the structure to undergo the chain rotations that break and form the new bonds associated with the symmetry changes of clinoamphiboles with smaller M4 site cations.

Metastable tremolite has been invoked as playing a primary role in both intermediate depth earthquakes and in generating conductivity anomalies at depths substantially deeper than its equilibrium stability within subduction zones (Scamburelli et al., 2017; Shen et al., 2020). Our results strongly indicate that tremolite should be stable in the *C2/m* space group throughout its persistence interval within the planet. Moreover, our results demonstrate that the elastic anisotropy of tremolite markedly decreases under compression: hence, calculations of the seismic anisotropy of mineral assemblages within subduction zones that are based on the zero-pressure elastic anisotropy of tremolite could markedly underestimate the amount of tremolite at depth. Our results further show that, at 300 K, tremolite has the largest known range of metastability of any amphibole, and that this metastability is likely generated by the role of large calcium cations in preventing the chain readjustments that generate phase transitions in other amphiboles.

Finally, we note that the interplay between the calcium ion's presence in tremolite and the inability of the tetrahedral chains to readjust likely produces a structural contretemps that has a likelihood of ultimately generating a structural instability (and possibly amorphization) at 300 K at pressures higher than ~39 GPa. As previously noted, tracking of single-crystal diffraction from tremolite proved impossible above this pressure due to the poor peak/background ratio of the diffraction data. This loss of intensity occurred within the quasi-hydrostatic pressure range of the neon pressure-medium with no visible damage to the tremolite single-crystal. Similar peak/background ratio degradation has been reported previously at high pressures in α-quartz by Hazen et al. (1989), where it was interpreted as the initial manifestation of an incipient crystal-amorphous transition in the sample. Our previous Raman results were able to track bands associated with tremolite to ~49 GPa (Ott and Williams, 2020), but the high sensitivity of single-crystal X-ray diffraction peaks to mosaic spread in the sample facilitates earlier observation of the onset of sample amorphization (Hazen et al., 1989). This evidence in conjunction with both the marked stiffening of our current elastic results in regime III and the marked decrease in most lattice mode shifts of tremolite in this pressure range between 39 and 49 GPa indicate that tremolite is likely approaching a lattice instability, even within a quasi-hydrostatic pressure medium.

Tremolite represents the Mg-rich endmember of the tremolite-actinolite-ferro-actinolite solid solution and it is thus interesting to consider the effect of increasing amounts of Fe^{2+} substitution for Mg^{2+} in the M1, M2, and M3 sites of actinolite and

ferro-actinolite. Any substitution of high-spin Fe^{2+} for Mg^{2+} in these octahedral sites results in an increase in size of the central cation in these units, which may in turn induce a structural instability at lower pressures. In an infrared spectroscopic study of the hydroxyl vibrations of amphiboles at high pressures (Thompson et al., 2016), the pressure shift of the hydroxyl B-band of actinolite decreases to a near-zero pressure-dependence above ~30 GPa, which is evocative of a saturation of the compression mechanism for this vibration. We speculate that increasing Fe^{2+} substitution on the tremolite-ferro-actinolite join carries with it the prospect of decreased metastability ranges for solid solutions with actinolite and ferro-actinolite, respectively.

Bibliography

Angel RJ (2000a) High-pressure structural phase transitions. Reviews in Mineralogy and Geochemistry 39: 85–104

Angel RJ (2000b) Equations of State. Reviews in Mineralogy and Geochemistry 41: 35-57

Apopei AI, Buzgar N (2010) The Raman study of amphiboles. Analele Ştiinţifice ale Universităţii "Al. I. Cuza" Iaşi, Geologie. LVI: 57–83

Arlt T, Angel RJ (2000) Displacive phase transitions in c-centered clinopyroxenes: spodumene, $LiScSi_2O_6$ and $ZnSiO_3$. Physics and Chemistry of Minerals 27: 719-731

Arlt T, Angel RJ, Miletich R, Armbruster T, Peters T (1998) High-pressure *$P2_1/c$-C2/c* phase transitions in clinopyroxenes: influence of cation size and electronic structure. American Mineralogist 83: 1176-1181

Bell DR, Rossman GR (1992) Water in Earth's mantle: The role of nominally anhydrous minerals. Science 255: 1391–1397

Birch F (1978) Finite strain isotherm and velocities for single-crystal and polycrystalline NaCl at high pressures and 300°K. Journal of Geophysical Research: Solid Earth 83: 1257–1268

Blaha JJ, Rosasco GJ (1978) Raman microprobe spectra of individual microcrystals and fibers of talc, tremolite, and related silicate minerals. Analytical Chemistry 50: 892–896

Boffa Ballaran T, Angel RJ, Carpenter MA (2000) High-pressure transformation behavior of the cummingtonite-grunerite solid solution. European Journal of Mineralogy 12: 1195-1213

Bradbury SE, Williams Q (2003) Contrasting bonding behavior of two hydroxyl-bearing metamorphic minerals under pressure: Clinozoisite and topaz. American Mineralogist 88: 1460-1470

Brown JM, Abramson EH (2016) Elasticity of calcium and calcium-sodium amphiboles. Physics of the Earth and Planetary Interiors 261: 161–171

Bruker (2016) APEX3. Madison, Wisconsin: Bruker AXS Inc. Software

Caracas R, Bobocioiu E (2011) The WURM project—a freely available web-based repository of computed physical data for minerals. American Mineralogist 96: 437–443

Comodi P, Mellini M, Ungaretti L, Zanazzi PF (1991) Compressibility and high-pressure structure refinement of tremolite, pargasite and glaucophane. European Journal of Mineralogy 3 (3): 485–499

Comodi P, Boffa Ballaran T, Zanazzi PF, Capalbo C, Zanetti A, Nazzareni S (2010) The effect of oxo-component on the high-pressure behavior of amphiboles. American Mineralogist 95: 1042-1051

Coppens P (1970) The evaluation of absorption and extinction in single crystal structure analysis. In F.R. Ahmed, S.R. Hall, and C.P. Huber, Eds., Crystallographic Computing, p. 255-270. Munksgaard, Copenhagen

Finkelstein GJ, Dera PK, Duffy TS (2015) Phase transitions in orthopyroxene (En90)

to 49 GPa from single-crystal X-ray diffraction. Physics of the Earth and Planetary Interiors 244: 78-86

Graham CM, Harmon RS, Sheppard SMF (1984) Experimental hydrogen isotope studies: Hydrogen isotope exchange between amphibole and water. American Mineralogist 69: 128-138

Gillet P, Hemley RJ, McMillan PF (1998) Vibrational properties at high temperatures and pressures. Reviews in Mineralogy and Geochemistry 37: 525-590

Gonzalez-Platas J, Alvaro M, Nestola F, Angel RJ (2016) EosFit7-GUI: A new GUI tool for equation of state calculations, analyses, and teaching. Journal of Applied Crystallography 49: 1377-1382

Hawthorne FC (1981) Crystal chemistry of the amphiboles. Reviews in Mineralogy and Geochemistry 9A: 1-102

Hawthorne FC, Grundy HD (1976) The crystal chemistry of the amphiboles: IV. X-ray and neutron refinements of the crystal structure of tremolite. The Canadian Mineralogist 14: 334-345

Hawthorne FC, Ventura GD (2007) Short-range order in amphiboles. Reviews in Mineralogy and Geochemistry 67: 173–222

Hazen RM, Finger LW, Hemley RJ, Mao HK (1989) High-pressure crystal chemistry and amorphization of α-quartz. Solid State Communications 72(5): 507-511

Hu Y, Kiefer B, Bina CR, Zhang D, Dera PK (2017) High-pressure g-CaMgSi2O6: Does penta-coordinate silicon exist in the Earth's mantle? Geophysical Research Letters 44: 11340- 11348

Huang E (2002) Raman spectroscopic study of amphiboles. Master Thesis, National Cheng Kung University, Taiwan

Jeanloz R (1988) Easy transformations in glasses. Nature 332: 207

Kawamoto T, Yoshikawa M, Kumagai Y, Mirabueno MHT, Okuno M, Kobayashi T (2013) Mantle wedge infiltrated with saline fluids from dehydration and decarbonation of subducting slab. Proceedings of the National Academy of Sciences 110: 9663–9668

Klotz S, Chervin JC, Munsch P, Le Marchand G (2009) Hydrostatic limits of 11 pressure transmitting media. Journal of Physics D: Applied Physics 42: 075413

Konzett J, Fei Y (2000) Transport and storage of potassium in the Earth's upper mantle and transition zone: An experimental study to 23 GPa in simplified and natural compositions. Journal of Petrology 41: 583-603

Krupka KM, Hemingway BS, Robie RA, Kerrick DM (1985) High-temperature heat capacities and derived thermodynamic properties of anthophyllite, diopside, dolomite, enstatite, bronzite, talc, tremolite, and wollastonite. American Mineralogist 70 (3-4): 261-271

Koziskova J, Hahn F, Richter J, Kožíšek J (2016) Comparison of different absorption corrections on the model structure of tetrakis (μ_2-acetato)-diaqua-di-copper(II). Acta Chimica Slovaca, 9(2): 136-140

Lafuente B, Downs RT, Yang H, Stone N (2015) The power of databases: the RRUFF project. In: Armbruster T, Danisi RM (ed) Highlights in

Mineralogical Crystallography, W. DeGruyter, Berlin, Germany pp 1-30

Law AD, Whittaker EJW (1980) Rotated and extended model structures in amphiboles and pyroxenes. Mineralogical Magazine 43: 565–574

Leake BE, Woolley AR, Arps CES, Birch WD, Gilbert MC, Grice JD, Hawthorne FC, Kato A, Kisch HJ, Krivovichev VG, Linthout K, Laird J, Mandarino JA, Maresch WV, Nickel EH, Rock NMS, Schumacher JC, Smith DC, Stephenson NCN, Ungaretti L, Whittaker EJW, Youzhi G (1997) Nomenclature of amphiboles; report of the subcommittee on amphiboles of the International Mineralogical Association commission on new minerals and mineral names. Mineralogical Magazine 61: 295-321

Lutz HD (1995) Hydroxide ions in condensed materials—correlation of spectroscopic and structural data. In: Mingos DMP (ed) Coordination Chemistry, Structure and Bonding, Springer, vol 82. Berlin, Heidelberg, pp 85-103

Mao HK, Xu J, Bell PM (1986) Calibration of the ruby pressure gauge to 800 kbar under quasi-hydrostatic conditions. Journal of Geophysical Research 91(B5): 4673-4676

Ott JN, Williams Q (2020) Raman spectroscopic constraints on compression and metastability of the amphibole tremolite at high pressures and temperatures. Physics and Chemistry of Minerals 47: 27

Papike JJ, Clark JR (1968) The crystal structure and cation distribution of glaucophane. American Mineralogist 53: 1156-1173

Papike JJ, Ross M (1970) Gedrites; crystal structures and intracrystalline cation

distributions. American Mineralogist 55 (11-12): 1945-1972

Parsons S (2010) ECLIPSE—Program for masking high-pressure diffraction images and conversion between CCD image formats. Software

Pawley AR, Holloway JR (1993) Water sources for subduction zone volcanism: New experimental constraints. Science 260: 664–667

Peng Y, Mookherjee M (2020) Thermoelasticity of tremolite amphibole: Geophysical implications, American Mineralogist (in press)

Poli S, Schmidt MW (1995) H_2O transport and release in subduction zones: Experimental constraints on basaltic and andesitic systems. Journal of Geophysical Research 100: 22299–22314

Poli S, Schmidt MW (2002) Petrology of subducted slabs. Annual Review of Earth and Planetary Sciences 30: 207–235

Prewitt CT, Papike JJ, Ross M (1970) Cummingtonite: A reversible, nonquenchable transition from $P2_1/m$ to C2/m symmetry. Earth and Planetary Science Letters 8: 448-450

Sakuyama M, Koyaguchi T (1984) Magma mixing in mantle xenolith-bearing calc-alkalic ejecta, Ichinomegata volcano, Northeastern Japan. Journal of Volcanology and Geothermal Research 22: 199–224

Savitsky A, Golay MJE (1964) Smoothing and differentiation of data by simplified least squares procedures. Analytical Chemistry 36(8): 1627-1639

Scamburelli M, Pennacchioni G, Gilio M, Bestmann M, Plumper O, Nestola F (2017) Fossil intermediate-depth earthquakes in subducting slabs linked to

differential stress release. Nature Geoscience 10: 960-966

Schmidt MW, Poli S (1998) Experimentally based water budgets for dehydrating slabs and consequences for arc magma generation. Earth and Planetary Science Letters 163: 361–379

Scott HP, Liu Z, Hemley RJ, Williams Q (2007) High-pressure infrared spectra of talc and lawsonite. American Mineralogist 92: 1814-1820

Serghiou G, Boehler R, Chopelas A (2000a) Reversible coordination changes in crystalline silicates at high pressure and ambient temperature. Journal of Physics: Condensed Matter 12: 849-857

Serghiou G, Chopelas A, Boehler R (2000b) Explanation of pressure-induced transformations in chain silicates based on their modular structures. Journal of Physics: Condensed Matter 12: 8939-8952

Sheldrick GM (2008) A short history of SHELX. Acta Crystallographica A64: 112-122

Shen K, Wang D, Liu T (2020) Electrical conductivity of tremolite under high temperature and pressure: Implications for the high-conductivity anomalies in the Earth and Venus. Contributions to Mineralogy and Petrology 175: 52.

Sheu JL, McMillan PF (1988) An ab initio study of the O-H stretching frequency in tremolite. Physics and Chemistry of Minerals 16: 114-119

Shinoda K, Aikawa N (1997) IR active orientation of OH bending mode in topaz. Physics and Chemistry of Minerals 24: 551-554

Shurvell HF, Rintoul L, Fredericks PM (2001) Infrared and Raman spectra of jade

and jade minerals. Internet Journal of Vibrational Spectroscopy 5 (5): 4

Stern RJ (2002) Subduction zones. Reviews of Geophysics 40(4): 1-38

Stoe, Cie (2009) X-Area V1.76 Software. Stoe & Cie GmbH, Darmstadt, Germany. Software

Sueno S, Papike JJ, Prewitt CT, Brown GE (1972) Crystal chemistry of high cummingtonite. Journal of Geophysical Research 77: 5767-5777

Sueno S, Cameron M, Papike JJ, Prewitt CT (1973) The high temperature crystal chemistry of tremolite. American Mineralogist 58 (7-8): 649-664

Tarling MS, Smith SAF, Scott JM (2019) Fluid overpressure from chemical reactions in serpentinite within the source region of deep episodic tremor. Nature Geoscience 12: 1034-1042

Thompson EC, Campbell AJ, Liu Z (2016) In-situ infrared spectroscopic studies of hydroxyl in amphiboles at high pressure. American Mineralogist 101: 706-712

Tribaudino M, Prencipe M, Nestola F, Hanfland M (2001) A *$P2_1/c$-C2/c* high-pressure phase transition in $Ca_{0.5}Mg_{1.5}Si_2O_6$ clinopyroxene. American Mineralogist 86: 807-813

Wang A, Dhamelincourt P, Turrell G (1988) Raman microspectroscopic study of the cation distribution in amphiboles. Applied Spectroscopy 42: 1442-1450

Whittaker EJW (1960) The crystal chemistry of the amphiboles. Acta Crystallographica A13: 291-298

Widulle F, Ruf T, Konuma M, Silier I, Cardona M, Kriegseis W, Ozhogin VI (2001) Isotope effects in elemental semiconductors: A Raman study of silicon. Solid

State Communications 118: 1–22

Williams Q (1992) A vibrational spectroscopic study of hydrogen in high pressure mineral assemblages. In: Syono Y, Manghnani MJ (ed) High-Pressure Research: Application to Earth and Planetary Sciences, vol 67. American Geophysical Union (AGU), pp 289-296

Williams Q, Knittle E, Scott HP, Liu Z (2012) The high-pressure behavior of micas: Vibrational spectra of muscovite, biotite, and phlogopite to 30 GPa. American Mineralogist 97: 241-252

Wong-Ng W, Siegrist T, DeTitta GT, Finger LW, Evans HT Jr., Gabe EJ, Enright GD, Armstrong JT, Levenson M, Cook LP, Hubbard CR (2001) Standard Reference Material (SRM 1990) for single crystal diffractometer alignment. Journal of Research of the National Institute of Standards and Technology 106(6): 1071–1094

Yang H, Evans BW (1996) X-ray structure refinements of tremolite at 140 and 295 K: Crystal chemistry and petrologic implications. American Mineralogist 81: 1117-1125

Yang H, Hazen RM, Prewitt CT, Finger LW, Lu R, Hemley (1998) High-pressure single-crystal X-ray diffraction and infrared spectroscopic studies of the *C2/m-P2₁/m* phase transition in cummingtonite. American Mineralogist 83: 288-299

Yang H, Prewitt CT (2000) Chain and layer silicates at high temperatures and pressures. Reviews in Mineralogy and Geochemistry 41: 211-255

Yang H, Smyth JV (1996) Crystal structure of $P2_1/m$ ferromagnesian cummingtonite at 140 K. American Mineralogist 81: 363-368

Yong T, Dera P, Zhang D (2019) Single-crystal X-ray diffraction of grunerite up to 25.6 GPa: a new high-pressure clinoamphibole polymorph. Physics and Chemistry of Minerals 46: 215-227